TITLE

Systematic identification of molecular mediators underlying sensing of *Staphylococcus aureus* by *Pseudomonas aeruginosa*

AUTHORS

Tiffany M. Zarrella[1, 2] and Anupama Khare[1, #]

[1]Laboratory of Molecular Biology, Center for Cancer Research, National Cancer Institute, National Institutes of Health, Bethesda, MD, USA

[2]Postdoctoral Research Associate Program, National Institute of General Medical Sciences, National Institutes of Health, Bethesda, MD, USA

[#]Address correspondence to anupama.khare@nih.gov

Running head: Sensing of *Staphylococcus aureus* by *Pseudomonas aeruginosa*

Key words: *Pseudomonas aeruginosa*, *Staphylococcus aureus*, interspecies sensing, staphylopine, zinc competition, intermediate metabolite, citrate, polymicrobial

The authors declare no conflict of interest.

ABSTRACT

Bacteria typically exist in dynamic, multispecies communities where polymicrobial interactions influence fitness. Elucidating the molecular mechanisms underlying these interactions is critical for understanding and modulating bacterial behavior in natural environments. While bacterial responses to foreign species are frequently characterized at the molecular and phenotypic level, the exogenous molecules that elicit these responses are understudied. Here we outline a systematic strategy based on transcriptomics combined with genetic and biochemical screens of promoter-reporters to identify the molecules from one species that are sensed by another. We utilized this method to study interactions between the pathogens *Pseudomonas aeruginosa* and *Staphylococcus aureus* that are frequently found in co-infections. We discovered that *P. aeruginosa* senses diverse staphylococcal exoproducts including the metallophore staphylopine, intermediate metabolites citrate and acetoin, and multiple molecules that modulate its iron starvation response. Further, we show that staphylopine inhibits biofilm formation and that *P. aeruginosa* can utilize citrate and acetoin for growth, revealing that these interactions have both antagonistic and beneficial effects. Our screening approach thus identified multiple *S. aureus* secreted molecules that are sensed by *P. aeruginosa* and affect its physiology, demonstrating the efficacy of this approach, and yielding new insight into the molecular basis of interactions between these two species.

INTRODUCTION

Bacteria frequently exist in multispecies communities in which cooperative and competitive interactions govern community composition and physiological outputs. Interactions among pathogenic bacterial species in multispecies infections can affect disease outcomes and antibiotic susceptibility (1, 2). Elucidating the molecules underlying these interactions is therefore critical to understand and modulate bacterial behavior in communities, and pairwise interaction studies using unbiased genetic and biochemical approaches are powerful tools for such analyses (3-5).

Previous studies on pairwise interspecies interactions have focused on the identification of molecules produced by one species and the effect of these molecules on specific phenotypes of another species, such as growth, biofilm formation, or antibiotic resistance (6-11). Recent work has described the genome-wide response of one species to another at the molecular level using either transcriptomics, proteomics, or metabolomics in multispecies conditions, revealing that these responses can be complex and affect numerous pathways (12-14), and are therefore likely mediated by multiple sensed secreted factors.

One powerful strategy to determine the cues being sensed by bacteria is to infer them from the cellular response. Examples include the SOS response indicating the sensing of DNA damage, or the heat shock response revealing the perception of high environmental temperature (15-17). In multispecies communities, specific bacterial responses have been used to identify the interspecific mediators. These include the upregulation of oxidative stress pathways in response to secreted redox-active molecules, alleviation of nutritional requirements due to sensing and use of secreted amino acids or other nutrients, and induction of iron starvation pathways by sensed iron competition caused by siderophores secreted by a foreign species (18-20). However, most such studies of interactions typically focus on a single response and the underlying molecules.

The goal of this work was to develop a comprehensive approach to define which exoproducts from one species are sensed by another and use this framework to study interspecies sensing in a model two-species system consisting of *Pseudomonas aeruginosa* and

Staphylococcus aureus. Both are opportunistic pathogens that co-exist in wound infections, nosocomial pneumonia, as well as lung infections in cystic fibrosis (CF) patients (21-24), where co-infection with both pathogens has been associated with increased disease severity (25-27). Identifying the molecular determinants of interactions between these two co-infecting pathogens can thus provide novel insights into persistent infections and multispecies communities in general.

Interactions between these two species have been extensively studied (reviewed by (28-31)). *P. aeruginosa* affects the growth, metabolism, antibiotic resistance, and transcriptional state of *S. aureus*, mainly via the secretion of multiple antimicrobials (6, 32-35). *S. aureus* induces exploratory motility in *P. aeruginosa* via unknown exoproducts, and the quorum sensing molecule autoinducer-2 and cell wall precursor *N*-acetyl glucosamine which can be produced by *S. aureus* affect the regulation of *P. aeruginosa* virulence factors (36-41). However, characterization of the *P. aeruginosa* transcriptional response to *S. aureus*, and the comprehensive identification of the underlying sensed *S. aureus* secreted factors and their production pathways, have not been fully accomplished.

In this study, we outline a strategy to systematically identify the secreted molecules from one species that are sensed by another, utilizing transcriptomics in conjunction with genetic and biochemical screens of promoter-reporters. Our approach revealed that *P. aeruginosa* senses four distinct signals secreted by *S. aureus*: the metallophore staphylopine (StP) which induces zinc starvation, the intermediate metabolites citrate and acetoin which induce their uptake and catabolism, and unidentified molecules that affect iron-related pathways. Through the genome-wide screen, we also delineate the *S. aureus* genes that alter the production of these sensed molecules. Further, we find that these staphylococcal exoproducts mediate both antagonistic and beneficial effects on *P. aeruginosa* physiology. StP participates in metal competition and abrogates *P. aeruginosa* biofilm formation, while the intermediate metabolites can serve as sole carbon sources, and the iron-chelating secreted factors deliver iron to *P. aeruginosa*. Clinical isolates of *S. aureus* show similar production of sensed molecules, and other bacterial species

can also induce some of the same pathways in *P. aeruginosa*, indicating the generality of these phenomena. Finally, we show that these *S. aureus* secreted molecules explain a major part of the *P. aeruginosa* response to *S. aureus*, demonstrating the utility of our approach to identify the secreted factors that underlie interspecies interactions.

RESULTS

Framework to comprehensively define the molecular mediators of bacterial interspecies sensing. We developed a systematic methodology within a two-species system to identify the sensed foreign molecules that underlie the global response of one species to the other **(Fig. 1A)**. Our approach first defines the complex response resulting from exposure to a foreign species and identifies the different individual components of the response. Then, these individual responses are used to identify the respective causal foreign molecules via unbiased genetic and biochemical screens. Unlike previous approaches, our strategy does not focus on the effect of individual molecules on a foreign species, or on globally identifying all molecules that are produced by a species, rather each response is used to identify the respective specific foreign molecules that together make up the interspecies interaction.

In the initial step, global transcriptional analysis is performed on one species exposed to another species or its cell-free supernatant compared to monocultures, to identify which pathways are differentially regulated by interspecies sensing. Next, promoter-reporter constructs are designed using representative genes from these upregulated classes. These promoter-reporter strains are then employed in two complementary approaches to identify the sensed interspecific molecules. First, an arrayed transposon mutant library in the species being sensed is screened to determine the mutants that are deficient in inducing reporter expression. The mutants are likely to be involved in the regulation, biosynthesis, or secretion of the cues, and mutant gene function is therefore used to identify the sensed molecules. Second, the sensed supernatant is fractionated to identify fractions that contain the active molecules inducing the promoters which can then be

further analyzed by additional fractionation and mass spectrometry. This two-pronged unbiased approach can thus exhaustively reveal the molecules that lead to complex responses in a foreign species, irrespective of which pathways and mechanisms constitute the response. We applied this scheme to study the *S. aureus* secreted products that are sensed by *P. aeruginosa*.

***P. aeruginosa* senses *S. aureus* secreted products and upregulates metal- and metabolite-related pathways.** We focused on the response of *P. aeruginosa* to *S. aureus* cell-free supernatant, as opposed to a co-culture model, since *P. aeruginosa* produces antimicrobials that may kill and lyse *S. aureus* cells (29, 42, 43), thus affecting the relative levels of staphylococcal secreted products that may be present. To determine the response of *P. aeruginosa* PA14 to *S. aureus* JE2, we performed RNA-seq on early-log phase *P. aeruginosa* cultures at 20 min, 1 h, and 2 h after the addition of 25% (v/v) *S. aureus* spent media or the same volume of media as a control. We found ~100-200 genes that were significantly differentially expressed between these two conditions at each timepoint **(Fig. 1B, Table S1, and S2).**

We identified the major pathways that are induced in *P. aeruginosa* upon sensing *S. aureus* molecules to define candidate promoters for the screening strategy **(Fig. 1A)**. First, we performed Gene Ontology (GO) enrichment analysis of the differentially regulated genes in *P. aeruginosa* after *S. aureus* exposure **(Table S3)**. The downregulated genes showed enrichment of amino acid metabolism genes while upregulated genes indicated significant enrichment in genes involved in metal ion transport, as well as the biosynthesis of the siderophore pyoverdine, suggesting the sensing of metal deprivation **(Fig. 1C and Table S3)**. Several genes previously reported to be controlled by the Zn-dependent repressor Zur, the Fe-dependent repressor Fur, and the Fe-specific sigma factor PvdS in *P. aeruginosa* PAO1 were upregulated 20 min after *S. aureus* supernatant exposure **(Fig. 1D and Table S4)** (44-46). Next, to identify additional robustly upregulated pathways that may not be well described by GO terms, we focused on all the upregulated genes that increased in fold change over time upon *S. aureus* supernatant exposure.

Of the 461 total upregulated genes, 73 increased over time across the three time points **(Fig. S1)**. We selected the operons that showed the highest terminal fold change, and these were associated with intermediate metabolite pathways, namely acetoin catabolism and tricarboxylic acids (TCA) uptake **(Fig. 1E and Fig. S1)**.

The strongest *P. aeruginosa* response to *S. aureus* cell-free supernatant was thus represented by four pathways: Zn-deprivation, Fe-deprivation, TCA uptake, and acetoin catabolism. We selected one promoter from each of these four pathways whose respective transcripts had distinct patterns of expression in the RNA-seq analysis (PA14_11320, *pvdG*, *opdH*, *acoR*, respectively) **(Fig. 2A)** and designed promoter-reporters using the fluorescent protein mScarlet. Each reporter led to significantly higher levels of mScarlet expression in the presence of *S. aureus* supernatant, displaying dose-dependent responses compared to the media control **(Fig. 2B)**. The two metal deprivation promoter-reporter strains induced the reporter earlier in the supernatant than the control, while the two intermediate metabolite reporter strains induced the reporter almost exclusively upon *S. aureus* supernatant exposure.

The metallophore activity of staphylopine upregulates the Zn-deprivation response in *P. aeruginosa*. Each promoter-reporter strain was used to screen supernatants from the Nebraska Transposon Mutant Library (NTML) which contains over 1,800 ordered transposon mutants in methicillin-resistant *S. aureus* JE2 (47). We reasoned that transposon insertions in the genes involved in the expression, biosynthesis, or export of the sensed product(s) would result in altered promoter induction.

Using the promoter of a putative lipoprotein under control of the Zur regulon (PA14_11320) (44) to screen the NTML for mutants that were deficient in inducing mScarlet reporter expression, we found candidates with transposon insertions in the genes encoding the exporter (*cntE*) or biosynthetic enzymes (*cntKLM*) of the multi-metal binding molecule staphylopine (StP) **(Fig. 3A, 3B, and Table S5)**. StP is a nicotianamine-like molecule that is exported out of the cell, where it

binds zinc and imports it back into the cell (48). StP is generated from L-histidine in three stepwise reactions by histidine racemase CntK, nicotianamine synthase CntL, and opine dehydrogenase CntM which incorporates pyruvate at the terminal step (48, 49). StP supports growth in zinc-deficient conditions, and mutants in the StP biosynthesis or export pathways show growth defects in the presence of the zinc chelator *N*,*N*,*N′*,*N′*-tetrakis(2-pyridinylmethyl)-1,2-ethanediamine (TPEN) **(Fig. S2A)** (50, 51).

P. aeruginosa produces a similar secreted opine metallophore, pseudopaline (PsP), that is also important for zinc uptake, and is produced by CntL and CntM with the addition of a terminal α-ketoglutarate instead of pyruvate **(Fig. 3A)** (49, 52-54). PsP is exported by CntI in the inner membrane and MexAB-OprM in the outer membrane and is imported back into the cell by CntO (52, 55). The entire *cntOLMI* operon was upregulated upon exposure to *S. aureus* supernatant **(Table S1 and S2)**. Along with P'PA14_11320, we examined StP-mediated induction of two other Zur-regulated promoters: *cntO* (PA14_63960), the first gene in the *cnt* operon, and *dksA2* (PA14_73020), which encodes a transcription factor in an operon with cobalamin synthesis genes (56). *S. aureus cnt* mutants lacking StP reduced mScarlet reporter expression from these three Zur-regulated promoters compared to wild type (WT) **(Fig. 3B)**. The addition of increasing amounts of StP to the *cntM*::tn mutant supernatant restored P'PA14_11320 induction to WT levels at concentrations greater than 40 µM **(Fig. 3C)**, indicating that similar concentrations are likely present in staphylococcal supernatant. Next, we sought to characterize if StP chelates metals from or delivers metals to *P. aeruginosa*. Addition of the zinc chelator TPEN increased promoter induction, with 0.5 µM mimicking the induction seen upon addition of *S. aureus* supernatant **(Fig. 3D and Fig. S2B)**. Inversely, the induction was decreased by the addition of zinc, cobalt, or nickel **(Fig. 3E and Fig. S2C)** suggesting that StP chelates these metals, thereby inducing the zinc starvation response in *P. aeruginosa*.

To examine the role of the similar *P. aeruginosa* opine metallophore PsP in the response to StP, induction of P'PA14_11320 was measured in *P. aeruginosa* mutants lacking the genes

encoding the importer (*cntO*), exporter (*cntI*), or entire *cnt* operon for PsP. Upon supernatant addition, induction of mScarlet reporter expression was increased in the Δ*cntO* and Δ*cnt* mutants compared to the WT **(Fig. 3F)**, demonstrating that the presence of PsP decreases StP-induced zinc starvation. Thus, in response to the opine metallophore StP, *P. aeruginosa* induces the Zur regulon which includes genes to synthesize its own zinc metallophore, PsP.

Higher levels of zinc availability are associated with increased *P. aeruginosa* biofilm formation and increased antagonism of *S. aureus* (57-59). We therefore explored the effects of StP, which we expect leads to zinc starvation, on *P. aeruginosa* biofilm formation and *P. aeruginosa*-*S. aureus* polymicrobial interactions. *P. aeruginosa* was grown in static conditions in medium with 0, 5, or 10 µM zinc added, and zinc addition increased biofilm formation **(Fig. 3G)**. While the addition of 1 or 2 µM TPEN had only modest effects on biofilm formation, 80 µM StP reversed the effects of zinc addition and inhibited biofilm formation **(Fig. 3G)**. A major component of *P. aeruginosa*-*S. aureus* interactions are *P. aeruginosa*-produced antimicrobials that inhibit *S. aureus* growth (29). To assess the role of StP on the inhibition of *S. aureus* growth by *P. aeruginosa*, cell-free supernatants were collected from *P. aeruginosa* cultures grown in 10 µM zinc, 1 µM TPEN, or 80 µM StP, and the growth of *S. aureus* in 50% (v/v) supernatant was determined. While supernatant from *P. aeruginosa* grown in zinc or TPEN inhibited *S. aureus* survival similar to the control, supernatant from *P. aeruginosa* cultured with StP showed lower inhibition of *S. aureus*, suggesting that StP may affect *P. aeruginosa* antimicrobial production **(Fig. S2D)**.

Staphylococcal secreted products affect siderophore-biosynthesis responses in *P. aeruginosa*. To determine the secreted products affecting the iron starvation response, the *S. aureus* transposon library was screened with the promoter of a pyoverdine synthesis gene, *pvdG*, which is induced by low-iron conditions (46). Since the *P. aeruginosa* Zur regulon was responding to a metallophore, we hypothesized that the *pvdG* promoter would similarly respond to a

siderophore but none of the *S. aureus* siderophore mutants reduced induction **(Table S6)**. Instead, we identified more than 100 mutants each that had a higher (upregulating) or lower (downregulating) induction of the reporter compared to the WT **(Fig. 4A and Table S6)**, and the relative iron chelation of the mutant supernatants did not correlate with their promoter induction (r = -0.04) **(Fig. 4B, S3A, and Table S7)**. Several downregulating supernatants had significantly higher chelation than WT, including those from mutants of the ATP-dependent proteases ClpC and ClpP, suggesting that these proteases contribute to the regulation of the chelating factor(s) **(Fig. 4B and Table S7)**.

It has been reported that *P. aeruginosa* can utilize specific iron-chelating xenosiderophores such as deferoxamine (DFX) to obtain iron (60-63), and P'*pvdG* was repressed by DFX **(Fig. S3B)**, showing iron delivery to *P. aeruginosa*. As a control, another iron chelator diethylene triamine penta-acetic acid (DTPA), which chelates iron away from *P. aeruginosa*, induced P'*pvdG* **(Fig. S3B)**. Thus, the lack of correlation between P'*pvdG* induction and relative chelation by the *S. aureus* mutant supernatants may be due to a combination of iron competition and delivery to *P. aeruginosa*.

Next, we employed the second approach in our strategy to determine the sensed secreted products **(Fig. 1A)** where we biochemically fractionated *S. aureus* supernatant by size-exclusion chromatography and then screened concentrated fractions for their ability to induce the P'*pvdG* promoter-reporter. We also treated each fraction with proteinase K to determine if the active molecule(s) contain peptide bonds. Relative to the water control, fraction 4 increased promoter induction, but this was abolished by proteinase K treatment, while fraction 5 only induced the promoter after proteinase K treatment **(Fig. 4C)**. Additionally, fractions 6-12 decreased induction regardless of proteinase K treatment **(Fig. 4C)**. Similar to our observations with the mutant supernatants, fraction 4 did not have any chelating activity, whereas the fractions that decreased promoter induction (fractions 6-12) did **(Fig. 4D).** This suggests that the chelators present in the

246 downregulating fractions repressed the expression of pyoverdine biosynthesis genes, possibly
247 due to delivery of iron to *P. aeruginosa*.

248 To test if secreted staphylococcal molecules could deliver iron to *P. aeruginosa*, we used
249 a *P. aeruginosa* Δ*pvdJ* Δ*pchE* mutant, which cannot produce the siderophores pyoverdine and
250 pyochelin. The Δ*pvdJ* Δ*pchE* mutant is unable to grow in medium containing 200 µM of the iron
251 chelator 2,2'-bipyridyl (BIP). The addition of DFX, but not DTPA, supports its growth in BIP media
252 **(Fig. S3C)**, confirming the ability of *P. aeruginosa* to utilize DFX to take up iron in the absence of
253 its own siderophores. Interestingly, the Δ*pvdJ* Δ*pchE* mutant grew in BIP media after addition of
254 whole *S. aureus* supernatant or individual fractions 5-12, but not media **(Fig. 4E and Fig. S3C)**.
255 Together with the promoter-reporter and iron chelation assays, these results indicate that one or
256 more *S. aureus* chelators deliver iron to *P. aeruginosa*, while at least one staphylococcal
257 exoproduct without chelating activity induces pyoverdine production.
258
259 ***S. aureus* secreted intermediate metabolites citric acid and acetoin induce uptake and**
260 **catabolism in *P. aeruginosa*.** To determine the staphylococcal secreted products that induce
261 expression of the TCA uptake operon, the NTML transposon collection was screened with the
262 *opdH* promoter-reporter strain. OpdH is a porin that uptakes TCAs, and is induced by the TCAs
263 isocitrate, cis-aconitate, and citrate (64). Similar to the screen with the *pvdG* promoter, we
264 obtained more than 100 mutants that upregulated or downregulated the *opdH* promoter **(Fig. 5A**
265 **and Table S8)**. GO enrichment analysis of these mutants indicated that aspartate family amino
266 acid biosynthesis genes were enriched in the upregulating mutants and branched-chain amino
267 acid biosynthesis, metabolism, and cellular respiration pathways were enriched in the
268 downregulating mutants **(Fig. 5B and Table S9)** (65-67). Many of the identified genes encode
269 proteins that catalyze enzymatic reactions within the TCA cycle and related pathways **(Fig. 5C,**
270 **Table S8, and Table S9)**. This included the downregulating supernatant from *gltA*::tn which
271 encodes citrate synthase II which converts TCA intermediates to citrate, and the upregulating

supernatant from *acnA*::tn encoding aconitate hydrase which breaks down citrate **(Fig. 5A and Table S8)**, suggesting that *S. aureus*-secreted citrate may induce the *opdH* promoter-reporter. Exogenously added citrate induced the P'*opdH* reporter in a dose-dependent manner with between 100-200 µM having similar induction to *S. aureus* supernatant **(Fig. 5D)**, and direct measurements showed that *S. aureus* supernatant contained 166.0 ± 13.0 µM citrate **(Fig. 5E and Table S10)**. Citrate concentrations in the upregulating and downregulating mutant supernatants significantly correlated with induction of the P'*opdH* promoter (Pearson's $r = 0.6663$, $p < 0.0001$) **(Fig. 5E and Table S10).** Therefore, *S. aureus* secretes the TCA intermediate metabolite citrate which is sensed by *P. aeruginosa*.

Recently, it was described that acetoin is released by *S. aureus* and in response, *P. aeruginosa* upregulates acetoin and butanoate pathways, including the *acoR* gene, which encodes a transcriptional regulator of the acetoin catabolism operon (68-70). We predicted that a transposon mutant screen of P'*acoR* induction may identify mutations in staphylococcal acetoin production and/or secretion. We identified nearly 200 mutants each that induced or repressed the promoter **(Fig. 6A and Table S11)**; however, no significant pathways were identified by GO enrichment analysis. Two of the most downregulating mutant supernatants had transposon insertions in *ilvB* and *ilvN*, which encode enzymes that convert pyruvate into α-acetolactate, leading into the butanoate cycle where acetoin and 2,3-butanediol are synthesized and catabolized **(Fig. 6A, C, and Table S11)**. The promoter of *acoR* is responsive to acetoin, 2,3-butanediol, and α-acetolactate, but not citrate **(Fig. 6B and Fig. S4A)**, however 2,3-butanediol and α-acetolactate could not be detected in *S. aureus* supernatant in quantities that would be needed to induce the promoter **(Fig. S4B)**. The acetoin concentration in the regulating mutant supernatants correlated with promoter induction in most supernatants (Pearson's $r = 0.2157$, $p < 0.0001$), including those of genes leading into the butanoate cycle **(Fig. 6C and D)**. However, a few select downregulating mutant supernatants contained significantly higher acetoin levels than WT, such as *sucD* encoding succinyl-CoA synthase and the *clpC* and *clpP* mutants **(Fig. 6D and**

298 **Table S12)**. Therefore, the main staphylococcal metabolite that induces *acoR* expression is
299 acetoin.

300 To ascertain if these intermediate metabolites can be utilized as carbon sources by *P.*
301 *aeruginosa*, 1 mM citrate, 2,3-butanediol, and/or acetoin, or 1 mM glucose as a positive control,
302 were added to the growth medium as the sole carbon source and *P. aeruginosa* growth was
303 monitored for 16 h. As expected, in the absence of any carbon sources, *P. aeruginosa* was unable
304 to grow (k = 0.003), while it grew with the addition of glucose (k = 1.057) **(Fig. 6E)**. *P. aeruginosa*
305 was also able to grow after addition of citric acid, 2-3-butanediol, and acetoin in combination (k =
306 0.781), or with just citric acid (k = 0.625), while slight growth was seen after the addition of 2,3-
307 butanediol or acetoin alone (k = 0.273 and 0.270) **(Fig. 6E)**. Thus, *P. aeruginosa* can utilize these
308 secreted intermediate metabolites as energy sources.
309
310 ***S. aureus* clinical isolates and other bacterial species also produce exoproducts that**
311 **induce *P. aeruginosa* response pathways.** Through the promoter-reporter screens, we
312 identified four distinct pathways in *P. aeruginosa* that are induced by *S. aureus* JE2 secreted
313 products. To test how widespread the production of these molecules is, we surveyed supernatants
314 from four clinical isolates of *S. aureus* that were mono-isolated (CF049 strain) or co-isolated with
315 *P. aeruginosa* (CF061, CF085, and CF089 strains) from cystic fibrosis patients. Supernatants
316 from these strains induced all four promoter-reporters in *P. aeruginosa* **(Fig. 7A)**, albeit to different
317 degrees. While all the strains contained chelators, only CF049 and CF061 supported siderophore-
318 deficient *P. aeruginosa* growth in iron-restricted medium **(Fig. 7B and C)**. CF089, which showed
319 the highest relative chelation, was unable to support the growth of the *P. aeruginosa* siderophore
320 mutant, indicating that *S. aureus* likely produces multiple chelators, only some of which can deliver
321 iron to *P. aeruginosa*, and the relative amounts of these may vary between strains. In addition,
322 citrate and acetoin concentrations in the supernatants largely correlated with induction of the

323 *opdH* and *acoR* promoters, respectively, except for CF061 and CF085 having lower levels of
324 acetoin **(Fig. 7D)**.

325 Since the sensing pathways in *P. aeruginosa* were induced by different strains of *S.*
326 *aureus*, we wondered if other bacterial species could also induce similar responses in *P.*
327 *aeruginosa*. Therefore, we tested cell-free supernatants from eight additional species: *Bacillus*
328 *subtilis*, *Staphylococcus epidermidis*, *Burkholderia cenocepacia*, *Escherichia coli*, *Klebsiella*
329 *pneumoniae*, *Salmonella enterica* Typhimurium, *Stenotrophomonas maltophilia*, and *Vibrio*
330 *cholerae*. Induction of the *P. aeruginosa* response pathways varied among the species, with
331 different combinations of two to four species inducing each pathway **(Fig. S5)**. Notably, *S.*
332 *epidermidis*, which is most closely related to *S. aureus*, did not induce zinc deprivation, pyoverdine
333 production, or *opdH* in *P. aeruginosa*, whereas *B. cenocepacia* induced all four promoters **(Fig.**
334 **S5)**.

335

336 **Identified secreted factors underlie a major part of the *P. aeruginosa* response to**
337 **staphylococcal exoproducts.** To determine if the identified molecules recapitulated the effect
338 of *S. aureus* whole supernatant on *P. aeruginosa*, we added the individual molecules or a
339 combination of all molecules to medium to *P. aeruginosa* cells and performed RNA-seq after 20
340 min and 2 h incubation **(Table S13)**. The molecules were added at concentrations measured from
341 the supernatant or that induced equivalent promoter activity: 80 µM StP, 150 µM citrate, and 150
342 µM acetoin. Since we did not identify the molecule(s) that induce the promoter of *pvdG*, we added
343 a mixture of the iron chelators DTPA and DFX at concentrations that represented the induction of
344 mScarlet reporter production **(Fig. S3B)**. The mixture of the two chelators was added to mimic
345 the dual phenotypes we observed, where DTPA induces the *pvdG* promoter, and DFX delivers
346 iron to *P. aeruginosa*. As expected, each of the four products induced the respective response
347 pathway in *P. aeruginosa* **(Fig. 8A)**. Compared to the medium control, addition of the supernatant,
348 the respectively paired identified products, or all products in combination led to upregulation of

the metal starvation genes PA14_11320 and *pvdG* at 20 min and intermediate metabolite uptake and metabolism genes *opdH* and *acoR* at 2 h **(Fig. 8A and Table S13)**. DTPA/DFX also induced PA14_11320, potentially due to chelation of zinc by DTPA **(Fig. 8A)** (71). We next determined what proportion of the *P. aeruginosa* response to *S. aureus* supernatant was explained by the identified products. Of the 417 genes that were upregulated upon exposure to *S. aureus* supernatant, 235 (56.3%) were also induced by at least one of the identified products, while 218 (52.3%) were induced upon exposure to the combination of all products **(Fig. 8B)**. Despite the sensed products being identified using upregulated promoter-reporters, of the 263 genes that were downregulated upon exposure to *S. aureus* supernatant, 133 (50.6%) were also repressed by at least one of the identified products, while the combination of all molecules downregulated 77 genes (29.3%) **(Fig. S6A)**. Thus, the four classes of identified sensed molecules account for a substantial part of both the upregulated and downregulated transcriptional responses of *P. aeruginosa* to *S. aureus* supernatant.

Given that we selected our promoter-reporters based on significantly enriched pathways and genes with high fold change of gene expression **(Fig. 1B and D)**, we posited that our identified sensed molecules likely underlie the upregulation of genes with higher fold change. In fact, the genes upregulated by both *S. aureus* supernatant and at least one of the identified molecules had a significantly higher fold change (mean $\log_2$(fold change) = 2.38) when compared to the genes that are solely induced by *S. aureus* supernatant (mean $\log_2$(fold change) = 1.50) **(Fig. 8C)**. For the downregulated genes, the overlapping genes had a significantly lower fold change (mean $\log_2$(fold change) = -1.83) when compared to the genes solely repressed by *S. aureus* supernatant (mean $\log_2$(fold change) = -1.33) **(Fig. S6B)**.

We determined which molecules explained what proportion of the response to staphylococcal supernatant by generating an UpSet plot to show intersections of upregulated genes in the supernatant with those among groups of the other conditions **(Fig. 8D and Fig. S6C and D for expanded UpSet plots)**. The largest intersections were between the shared

upregulated genes after addition of the combination of all molecules and the iron chelators DTPA/deferoxamine (130 genes), and these conditions and StP (42 genes) **(Fig. 8D)**. These comparisons indicate that many of the genes induced by *S. aureus* supernatant are due to effects of exoproducts that induce iron-related pathways as well as zinc starvation, however intersections were found between the upregulated genes in *S. aureus* supernatant and each of the other conditions, showing their contribution to inducing distinct sensing pathways in *P. aeruginosa*. Taken together, we describe a model where *P. aeruginosa* senses the secreted staphylococcal molecules StP, iron chelators and unidentified proteins, and intermediate metabolites, and upregulates metal starvation pathways, thereby producing PsP and pyoverdine, and metabolite uptake and catabolism pathways to use citrate and acetoin as carbon sources **(Fig. 8E)**.

DISCUSSION

In this study, we developed a systematic unbiased strategy using transcriptomics combined with genetics to determine the secreted exoproducts from one species that can be sensed by another in a model two-species system. We used this approach to study the sensing of *S. aureus* by *P. aeruginosa*. Unlike other strategies that focus on a single molecule or response pathway of interest, our genome-scale approach revealed multiple staphylococcal factors that are sensed by *P. aeruginosa*, illustrating that interactions even between just two species can be complex and mediated by diverse molecules **(Fig. 8E)**. Our genome-wide screen also determined the mutations in *S. aureus* that affect the regulation, biosynthesis, and/or secretion of the sensed exoproducts. The sensed molecules we identified explain most of the *P. aeruginosa* transcriptional response to *S. aureus* in our system, suggesting that this systematic genome-wide approach can be applied to other two-species systems to comprehensively identify the underlying molecules that affect bacterial sensing in multispecies communities.

P. aeruginosa and *S. aureus* are commonly co-isolated from lung infections in CF patients and together contribute to worse disease outcomes compared to mono-infections (26, 27). It is

401 therefore imperative to better understand their interactions and the molecular mediators involved.
402 Here we found that *P. aeruginosa* senses multiple distinct *S. aureus* secreted molecules: the
403 metallophore StP which affects zinc starvation and biofilm formation, unidentified molecules that
404 affect pyoverdine production and/or deliver iron to *P. aeruginosa*, and the intermediate
405 metabolites citrate and acetoin which are carbon sources for *P. aeruginosa*. Further, production
406 of the sensed molecules was conserved in clinical isolates of *S. aureus* suggesting that these
407 pathways and interactions are common between these two species.

408 Staphylococcal exoproducts affected *P. aeruginosa* metal homeostasis, and zinc and iron
409 chelators defined >45% of the transcriptional response to *S. aureus* supernatant **(Fig. 8D, Fig.**
410 **S6, and Table S13)**. Zinc availability is required for virulence traits in both species, affecting *P.*
411 *aeruginosa* motility, biofilm formation, and protease activity (58, 59, 72-74) and *S. aureus* biofilm
412 formation and growth *in vivo* (50, 75-77). Interactions between *P. aeruginosa* and *S. aureus* in
413 the context of zinc deprivation have been studied before in the presence of a neutrophil-derived
414 metallophore, calprotectin, which binds zinc, manganese, nickel, and iron. Through metal
415 chelation, calprotectin decreases anti-staphylococcal antimicrobial production and inhibits
416 extracellular protease-mediated lysis of *S. aureus* thereby promoting coexistence between *P.*
417 *aeruginosa* and *S. aureus* (57, 58). Moreover, it has been shown that the availability of zinc affects
418 interactions between *P. aeruginosa* and the oral commensal species *Streptococcus sanguinis*
419 SK36, likely due to zinc sequestration by *P. aeruginosa* (78). We found that *S. aureus*-secreted
420 StP led to the upregulation of the biosynthesis genes of the metallophore PsP as well as other
421 components of the Zur-dependent zinc starvation response in *P. aeruginosa* due to reduced
422 availability of zinc. Additionally, StP inhibited *P. aeruginosa* biofilm formation and reduced *P.*
423 *aeruginosa* antimicrobial killing of *S. aureus*. Our screen thus revealed a new interaction between
424 *S. aureus* and *P. aeruginosa* through competition for and modulation of zinc availability by
425 microbial opine metallophores. Zinc deprivation genes in *P. aeruginosa* are known to be induced

426 in CF sputum (79-81), and our data suggest that competition with *S. aureus* may contribute to the
427 induction.

428 *P. aeruginosa* and *S. aureus* are thought to compete for limited iron availability during
429 infection via the secretion of iron-chelating siderophores and various iron uptake systems (28,
430 82). However, other studies have shown a downregulation of the *P. aeruginosa* iron starvation
431 response in the presence of *S. aureus* or cell-free supernatant (35, 70, 83) and lysis of *S. aureus*
432 liberates intracellular iron for acquisition by *P. aeruginosa* (35). The differences between studies
433 could be due to variability in the iron content of the culture media as well as the *S. aureus* strains
434 used. The results of our work support a complex effect of *S. aureus* on the *P. aeruginosa* iron
435 response where on the whole *S. aureus* secreted products led to an induction of *P. aeruginosa*
436 iron starvation responsive Fur- and PvdS-regulons, but *P. aeruginosa* obtains iron from specific
437 staphylococcal chelators through xenosiderophore piracy, iron acquisition via uptake of a foreign
438 siderophore (84). Characterization of this intriguing iron piracy, and identification of the likely novel
439 underlying molecules, will be the subject of a future study.

440 Through the transposon screen with P'*pvdG*, we also described the mutations in *S. aureus*
441 that affect production of these molecules and hence iron-responsive pathways in *P. aeruginosa*,
442 including in genes encoding metabolic enzymes, transcriptional regulators, and proteases.
443 Particularly, supernatant from *S. aureus clpP* and *clpC* mutants led to decreased *pvdG* promoter
444 induction, but a large increase in relative chelation **(Fig. 4B)**. Clp proteases comprise the main
445 proteolytic system in *S. aureus* and are known to affect iron homeostasis (85, 86), and our data
446 reinforce the idea that some *S. aureus* iron-related molecules may be direct or indirect targets of
447 the Clp proteolysis machinery.

448 Our results also define a syntrophic relationship between *P. aeruginosa* and *S. aureus*
449 where staphylococcal secreted intermediate metabolites citrate and acetoin can be used as
450 carbon sources by *P. aeruginosa*. Costless secretion of valuable metabolites, especially of
451 organic acids, is predicted to enable positive interspecies interactions through cross-feeding (87).

It was reported previously that *P. aeruginosa* can take up both metabolites as carbon sources (64, 70, 88, 89), and acetoin was recently identified to participate in this cooperative interaction between *P. aeruginosa* and *S. aureus* in clinical co-isolates (70), which validates our screening approach in determining sensed exoproducts. Extracellular citrate has been detected in *S. aureus* cultures previously (90, 91), and our work shows that this staphylococcal secreted metabolite can be sensed by *P. aeruginosa*, thus defining another cooperative interaction between these two co-infecting pathogens. Higher concentrations of citrate affect quorum sensing and biofilm formation, and mediate iron uptake in *P. aeruginosa* (60, 92, 93). While citrate did not affect iron pathways in our study at the concentration found in *S. aureus* JE2 supernatant **(Table S13)**, it is possible that higher concentrations that facilitate iron uptake may exist in communities with these two species. Our genome-wide screen identified mutations in *S. aureus* that affect production and/or secretion of these sensed intermediate metabolites, which is not only important for better understanding these cooperative interspecies interactions and general metabolism but also has implications for the effects of these metabolites on *S. aureus* such as acetoin affecting stress resistance or citrate influencing virulence (91, 94).

Previous studies have identified additional molecules that can be secreted by *S. aureus*, and are sensed by *P. aeruginosa*, such as *N*-acetyl glucosamine which induces the *nag* operon and autoinducer-2 which induces several virulence genes (36, 39, 95). However, these products were not identified during *S. aureus* co-culture and/or incubation with *S. aureus* supernatant, but rather with Gram-positive bacterial communities. We did not see these response pathways being induced in our study upon exposure to *S. aureus* cell-free supernatant, possibly due to differences in growth medium, experimental conditions, and timing of gene expression measurements between the studies, and/or insufficient amounts of these products being present in 25% (v/v) *S. aureus* supernatant.

There are limitations and considerations to using our screening approach. First, our study was conducted in a defined medium to avoid introduction of molecules from another species into

the two-species system, such as culture media compositions that contain whole cell lysates, and it is important to consider that culture and growth conditions may affect either secreted molecule production and/or sensory responses. Next, the species being studied must have the necessary genetic tools available, such as reporter expression systems and random mutagenesis protocols, however these are becoming more widely accessible (96-98). The identification of sensed products using our approach was more straightforward when there was a primary sensory molecule driving the response, such as in the case of StP, citrate, or acetoin, although fractionation of WT and mutant supernatants can reveal the molecules underlying multifactor-driven responses as well. Another consideration is that there is significant strain to strain variability in bacteria, and studies should therefore utilize a panel of strains to interrogate interspecies sensing. While our screen was carried out in a single strain of each species, we validated that *S. aureus* clinical isolates from cystic fibrosis patients, including strains that were co-isolated with *P. aeruginosa*, retained production of molecules that induced the sensory pathways, albeit at varying levels.

Studies of interactions between *P. aeruginosa* and *S. aureus* have often focused on the effects of *P. aeruginosa* antimicrobials on staphylococcal growth and survival, however it is an active question if these species, which are often co-isolated, are more prone to competition or coexistence (31). Here by identifying the staphylococcal secreted products that are sensed by *P. aeruginosa*, we uncovered instances of both aspects: competition for metals, siderophore piracy, lifestyle alteration via inhibition of biofilm formation, and cooperation through release of intermediate metabolites used as carbon sources. Altering the production of these factors could potentially tip the balance in favor of a more beneficial or antagonistic interaction between these species.

MATERIALS AND METHODS

Bacterial strains and growth conditions.

Bacterial strains utilized in this study are listed in **Table S14**. *P. aeruginosa* UCBPP-PA14 (99) and *S. aureus* JE2 (47), other species listed, and their derivatives were grown in a modified M63 medium (100) (13.6 $g \cdot L^{-1}$ KH_2PO_4, 2 $g \cdot L^{-1}$ $(NH_4)_2SO_4$, 0.8 µM ferric citrate, 1 mM $MgSO_4$; pH adjusted to 7.0 with KOH) supplemented with 0.3% glucose, 1× ACGU solution (Teknova), 1× supplement EZ (Teknova), 70 $ng \cdot L^{-1}$ biotin, and 7 $mg \cdot L^{-1}$ nicotinamide, at 37°C, shaken at 300 rpm, except where noted. *Vibrio cholerae* was grown in M63 with the addition of 2% NaCl. For *P. aeruginosa* Δ*pvdJ* Δ*pchE* growth assays, 200 µM 2,2'-bipyridyl (BIP) (Sigma Aldrich) was added to M63 medium. For sole carbon source growth assays, EZ and glucose were not added in the formulation. For each growth assay, *P. aeruginosa* overnight cultures were diluted to an OD_{600} of 0.05 before monitoring growth. The Nebraska Transposon Mutant Library (NTML) made up of 1,920 arrayed *bursa aurealis* transposon insertions in *S. aureus* JE2 was utilized for the transposon screen (47). For cloning and strain construction, strains were routinely cultured in Luria Bertani (Miller) broth or on agar plates with 20 $g \cdot L^{-1}$ agar. For selection, antibiotics were added as 50 $\mu g \cdot mL^{-1}$ gentamicin, 25 $\mu g \cdot mL^{-1}$ irgasan, 50 $\mu g \cdot mL^{-1}$ carbenicillin, and/or 10 $\mu g \cdot mL^{-1}$ erythromycin as needed. Other additives include staphylopine (Santa Cruz Biotechnology), TPEN (Sigma Aldrich), $ZnSO_4 \cdot 7H_2O$ (Sigma Aldrich), $NiCl_2 \cdot 6H_2O$ (J. T. Baker Chemical Company), $CoCl_2 \cdot 6H_2O$ (Sigma Aldrich), DTPA (Sigma Aldrich), deferoxamine mesylate salt (Sigma Aldrich), and intermediate metabolites citric acid (Sigma Aldrich), acetoin (Sigma Aldrich), 2,3-butanediol (98% (v/v) solution, Sigma Aldrich), and (S)-α-acetolactic acid potassium salt (Toronto Research Chemicals).

Preparation of *S. aureus* cell-free supernatant.

Overnight cultures of *S. aureus* strains were diluted to OD_{600} of 0.05 in fresh media and grown for 24 h in flasks (or tubes or 96-well plates for NTML library supernatant preparation). Bacterial

cultures grown in flasks were centrifuged at 4000 rpm for 20 minutes. The supernatant was applied to a Steriflip unit with a 0.2 µm polyethersulfone filter (MilliporeSigma). For supernatants prepared from the NTML library in 1-mL tube cultures or 96-well plates, culture was directly transferred to AcroPrep Advance 96-well 0.2 µm polyethersulfone filter plates (Pall) and centrifuged at 4000 rpm for 10 min to collect the sterile-filtered flow through. Supernatants were stored at -30°C until use.

RNA extraction and library preparation.

P. aeruginosa overnight cultures were diluted to OD_{600} of 0.05 in fresh media in flasks and grown to OD_{600} of 0.50. Two milliliters were collected for RNA extraction immediately before addition of 5 mL (25% v/v) of either fresh media, supernatant, or additives in media and collected after 20 min, 1 h, and 2 h for the data described in Fig. 1 and after 20 min and 2 h for the data described in Fig. 8. Removed culture was mixed with 4 mL of RNAprotect Bacteria Reagent (Qiagen) for stabilization and incubated for 5 min at room temperature before centrifugation at 4000 rpm for 10 min. Supernatants were completely removed before storage of the pellets at -80°C. RNA was extracted using the Total RNA Purification Plus Kit (Norgen) according to the manufacturer's instructions for Gram-negative bacteria. The extracted RNA was subjected to an additional genomic DNA removal by DNase I treatment in solution using the TURBO DNA-free Kit (Invitrogen) and checked by PCR for the absence of contaminating DNA. Integrity of the RNA preparation was confirmed by running on an agarose gel and observing intact rRNA bands. Next, rRNA was removed using the Ribo-Zero Depletion Kit for Gram Negative Bacteria (Illumina) or riboPOOLs (siTOOLs Biotech) before library preparation with the NEBNext Ultra II Directional RNA Library Prep Kit for Illumina (New England Biolabs). The sequencing was performed at the Center for Cancer Research Genomics Core Facility. Two biological replicates were performed.

RNA-seq analysis.

The sequencing files were processed with Cutadapt (101) and Trimmomatic (102). Alignment to the *P. aeruginosa* UCBPP-PA14 genome (NCBI) and pairwise comparisons were made using Rockhopper (Wellesley College) (103, 104). Upregulated and downregulated genes were based on transcripts that had $p < 0.05$ and $\log_2$ fold change ≥ or ≤ 1. Venn diagrams were generated using matplotlib_venn package with venn3 using Python (105). All upregulated genes were evaluated for increasing fold change over time. UpSet plots were generated with ComplexUpset using R (106). For UpSet plots, all upregulated genes at 20 min and 2 h were combined and compared between datasets.

Construction of *P. aeruginosa* promoter-reporter strains and mutants.

Bacterial strains and plasmids are listed in **Table S14**. Promoter sequences were amplified using the primers listed in **Table S15.** The amplified fragments were cloned by Gibson Assembly (NEB) into SpeI- and XhoI-digested pSEK109 (pLB3208), provided by the Dietrich lab (107). Plasmids were transformed into *E. coli* S17-1 λ-pir and confirmed by sequencing. Next, bi-parental conjugations were conducted as described previously between *E. coli* donor cells and *P. aeruginosa* recipients (20). For each conjugation, cells were collected and plated on LB + irgasan + gentamicin plates. The integration was then unmarked using Flp-FRT recombination by mating with an *E. coli* donor strain harboring the pFLP2 plasmid, selecting on LB + irgasan + carbenicillin, and further curing of this plasmid by selecting on LB plates (without NaCl) + 10% sucrose (108). All promoter-reporter strains were confirmed by PCR with the forward primer for the promoter and the reverse primer internal to mScarlet Pa094. For mutant construction, homologous downstream and upstream arms of *cnt* genes were amplified using the primers listed in **Table S15**. The amplified fragments were cloned into pDONRPEX18Gm *attP* sites using the Gateway BP Clonase II Enzyme mix (ThermoFisher). Plasmids were transformed into *E. coli* S17-1 λ-pir and confirmed by sequencing prior to conjugation as described above. Conjugants were streaked onto LB plates

582 (without NaCl) + 10% sucrose, and then tested for gentamicin resistance. Gentamicin-sensitive
583 strains were tested for the deletion by PCR and sequencing.
584
585 **Plate reporter assay.**
586 *P. aeruginosa* overnight cultures were diluted to OD_{600} of 0.05 in fresh media in flasks and grown
587 to OD_{600} of 0.5. At this time, 150 µL of culture was added to wells of a 96-well clear, flat-bottom
588 polystyrene plate with 50 µL fresh media (control) or *S. aureus* supernatant with or without
589 additives as described. Plates were incubated at 37°C with continuous orbital shaking at 807
590 cycles per minute (cpm) in a Synergy H1 microplate reader (BioTek) with fluorescence and optical
591 density measurements every 30 minutes (mScarlet: 565 nm excitation and 600 nm emission;
592 pyoverdine: 405 nm excitation and 460 nm emission (109); optical density at 600 nm).
593 Measurements for duplicate wells were averaged, and the fluorescence was normalized to the
594 growth (relative fluorescence units divided by the OD_{600}). Slopes were calculated from 1.5-5 h
595 (promoters of PA14_11320, *cntO*, PA14_73020, *opdH*, and *acoR*) or 1-4 h (promoter of *pvdG* and
596 pyoverdine).
597
598 **Gene ontology (GO) enrichment analysis.**
599 For *P. aeruginosa* PA14 pathway analysis, the open reading frame designations for the
600 corresponding PAO1 orthologs of *P. aeruginosa* UCBPP-PA14 genes were obtained using the
601 *Pseudomonas* Genome Database (www.pseudomonas.com/rbbh/pairs) (110). Similarly, for *S.*
602 *aureus* JE2 pathway analysis, the open reading frame designations for the corresponding
603 NCTC8325 orthologs of *S. aureus* JE2 USA300_FPR3757 genes were obtained using the
604 AureoWiki repository (http://aureowiki.med.uni-griefswalk.de/Downloads) (111). The list of
605 designations from the RNA-seq analysis (*P. aeruginosa*) or selected transposon mutants (*S.*
606 *aureus*) were analyzed at the Gene Ontology Resource (www.geneontology.org) by the
607 PANTHER Overrepresentation Test (released 20210224) (Annotation Version and Release Date:

608 GO Ontology database DOI: 10.5281/zenodo.5228828 Released 2021-08-18) or (released
609 20200728) (Annotation Version and Release Date: GO Ontology database DOI:
610 10.5281/zenodo.4081749 Released 2020-10-09), respectively, for enriched biological processes
611 by Fisher's exact test with Bonferroni correction.
612
613 **Biochemical fractionation.**
614 Five milliliters of *S. aureus* supernatant were frozen and lyophilized before resuspension in 500
615 µL of filtered water. The resuspension was separated using a Superdex 30 10/300 GL size
616 exclusion column (GE Healthcare) with filtered water as buffer at a flow rate of 0.7 $mL \cdot min^{-1}$ for
617 1.5 column volumes at 2.6 MPa for a total of 36.5 mL with 18 fractions collected after every 2 mL.
618 Fractions were frozen, lyophilized, and resuspended in 500 µL of water. For protease digestion,
619 60 µL of each fraction was treated with 1 µL of thermolabile proteinase K (New England Biolabs)
620 for 1 h at 37°C followed by inactivation for 10 min at 55°C.
621
622 **Biofilm formation assay.**
623 *P. aeruginosa* was grown overnight in modified M63 medium. Overnight culture was diluted to a
624 starting OD_{600} of 0.05 in fresh medium mixed with the indicated additives as described. One
625 hundred µL of culture was added to eight replicate wells of a 96-well plate. Biofilms were allowed
626 to form in static conditions for 24 h at 37°C and assessed for biofilm formation using crystal violet
627 staining (112).
628
629 **Supernatant survival assay.**
630 To prepare cell-free supernatant, *P. aeruginosa* was inoculated from an overnight culture at an
631 OD_{600} of 0.05 and allowed to grow for 16 h in medium with the indicated additives. The culture
632 was centrifuged, and the supernatant was filtered with a Steriflip unit with a 0.2 µm
633 polyethersulfone filter (MilliporeSigma). For the survival assay, *S. aureus* was inoculated from an

634 overnight culture at an OD_{600} of 0.05 and grown to an OD_{600} of 0.5. Next, 500 µL of culture was
635 added to 500 µL (50% v/v final concentration) of either *P. aeruginosa* cell-free supernatant or M63
636 salts control. After 16 h, *S. aureus* was plated on LB agar plates and enumerated after growth.
637
638 **Chromeazurol S (CAS) assay for iron chelation.**
639 Solutions were prepared exactly as described and assay was performed as described with some
640 changes (113). One hundred microliters of M63 media reference or 75 µL M63 with 25 µL of *S.*
641 *aureus* supernatant (1X concentration) were added to plate and mixed with 100 µL CAS shuttle
642 solution. Plates were incubated for 1 h at room temperature. The absorbance was measured at
643 OD_{630}. The absorbance ratio was calculated by dividing the average absorbance for the sample
644 by the absorbance of the media reference. Next, this ratio was normalized to a standard log-
645 based curve of WT supernatant to return the relative chelation.
646
647 **Citrate measurements.**
648 Citrate concentrations were measured in *S. aureus* supernatant using the Citric Acid Assay Kit
649 (Megazyme) according to the microplate assay instructions. Absorbances after the enzymatic
650 reaction were compared to a standard log-based curve of citric acid concentrations to determine
651 the concentration in supernatant.
652
653 **Acetoin and α-acetolactate measurements.**
654 Acetoin was measured by the Voges-Proskauer test adapted for microtiter plates essentially as
655 described (70, 114). In order, 35 µL 0.5% (m/v) creatine (Sigma), 50 µL 5% (m/v) α-naphthol
656 (Sigma), 50 µL 40% (v/v) KOH, and 50 µL *S. aureus* supernatant was added to each well. The
657 reaction was incubated at room temperature for 15 min and absorbance was measured at OD_{560}.
658 Concentrations were calculated based on a linear standard curve. To quantify α-acetolactate, 5 µl
659 2M H_2SO_4 was added to supernatant and incubated for 15 min at 60°C for decarboxylation of α-

660 acetolactate to acetoin before adding to the above reagents as described (115). Due to
661 precipitation in the wells, each mixture was transferred to a new well before reading absorbance.
662
663 **Quantification of 2,3 butanediol by mass spectrometry.**
664 Stock solution of 50 mM 2,3-butanediol (Sigma Aldrich) and calibration standards from 0 to 40
665 µM were prepared in water. The isotopic standard (IS) solution of 5 µM 2,3-butanediol (Toronto
666 Research Chemicals) was prepared in water. 2,3-Butanediol in the samples were determined by
667 LC-MS/MS after derivatization with trichloroacetyl isocyanate (Sigma Aldrich) according to Chen
668 et al. (116) with slight modification. In a 1.5 mL plastic vial, 5 µL of standard or sample was mixed
669 with 5 µL IS, 250 µL acetonitrile and 20 µL trichloroacetyl isocyanate. After 5 min, 250 µL water
670 was added to the vials and the mixture were analyzed by liquid chromatography-mass
671 spectrometry LC-MS/MS. LC were performed with a Shimadzu 20AC-XR system with a 2.1 x 100
672 mm, Cortecs C8 column (Waters). Mobile phase A was 10 mM ammonium formate with 0.15%
673 (v/v) formic acid in water and mobile phase B was methanol. The flow rate was 300 $\mu L \cdot min^{-1}$ and
674 the injection volume was 5 µL. 2,3-Butanediol was eluted from the column using a gradient (0-0.2
675 min/55% (v/v) B; 5 min/70% (v/v) B; 5.1-6 min/95% (v/v) B; 6.1-8 min/55% (v/v) B). MS/MS was
676 performed with a TSQ Vantage triple quadrupole mass spectrometer (Thermo Fisher Scientific)
677 operating in selected reaction monitoring mode with positive ionization. The derivatized peaks
678 were detected using the following mass-to-charge ratio (*m/z*) precursor > product ions: 2,3-
679 butanediol (484 > 262); 2,3-butanediol-d8 (492 > 270). 2,3-Butanediol concentrations in the
680 samples were determined by a linear calibration curve with 1/x weighting generated by the
681 Thermo Xcalibur software. The curve was constructed by plotting the peak area ratios vs.
682 standard concentrations. The peak area ratio was calculated by dividing the peak area of 2,3-
683 butanediol by the peak area of the IS.
684
685

686 **Accession number(s).**

687 The RNA-seq data have been deposited at NCBI Gene Expression Omnibus (GEO)
688 (https://www.ncbi.nlm.nih.gov/geo/) under accession numbers GSE185963 and GSE186138.

689

690 **ACKNOWLEDGMENTS**

691 We would like to acknowledge the Center for Cancer Research Genomics Core for RNA-
692 sequencing, King Chan at the Protein Characterization Laboratory at Frederick National
693 Laboratory for Cancer Research for quantifying 2,3-butanediol, the Cystic Fibrosis Foundation
694 Isolate Core for providing clinical isolate strains, and the Dietrich lab (Columbia University) for
695 providing the pSEK109 (pLD3208) plasmid. We thank Susan Gottesman, Kumaran Ramamurthi,
696 Gisela Storz, and Saaed Tavazoie for comments on the manuscript, and members of the
697 Gottesman, Ramamurthi, and Khare labs for discussion and feedback throughout this study. This
698 work utilized the computational resources of the NIH High Performance Computing Biowulf cluster
699 (http://hpc.nih.gov). Diagrams in Figures 1, 3, 5, and 8 were created with BioRender
700 (http://biorender.com). This work was supported by the Intramural Research Program of the NIH,
701 National Cancer Insitute, Center for Cancer Research. TMZ was supported by a Postdoctoral
702 Research Associate Training (PRAT) Fellowship award 1FI2GM137843-01 from the National
703 Institute of General Medical Sciences.

704

705 **COMPETING INTERESTS**

706 No competing interests declared.

REFERENCES

1. Tavernier S, Crabbe A, Hacioglu M, Stuer L, Henry S, Rigole P, Dhondt I, Coenye T. 2017. Community composition determines activity of antibiotics against multispecies biofilms. Antimicrob Agents Chemother 61:e00302–e00317.

2. Vandeplassche E, Tavernier S, Coenye T, Crabbe A. 2019. Influence of the lung microbiome on antibiotic susceptibility of cystic fibrosis pathogens. Eur Respir Rev 28:190041.

3. Little AE, Robinson CJ, Peterson SB, Raffa KF, Handelsman J. 2008. Rules of engagement: interspecies interactions that regulate microbial communities. Annu Rev Microbiol 62:375-401.

4. Khare A. 2021. Experimental systems biology approaches reveal interaction mechanisms in model multispecies communities. Trends Microbiol doi:10.1016/j.tim.2021.03.012.

5. Stubbendieck RM, Vargas-Bautista C, Straight PD. 2016. Bacterial communities: interactions to scale. Front Microbiol 7:1234.

6. Radlinski L, Rowe SE, Kartchner LB, Maile R, Cairns BA, Vitko NP, Gode CJ, Lachiewicz AM, Wolfgang MC, Conlon BP. 2017. *Pseudomonas aeruginosa* exoproducts determine antibiotic efficacy against *Staphylococcus aureus*. PLoS Biol 15:e2003981.

7. Dean SN, Chung MC, van Hoek ML. 2015. *Burkholderia* diffusible signal factor signals to *Francisella novicida* to disperse biofilm and increase siderophore production. Appl Environ Microbiol 81:7057-66.

8. Vega NM, Allison KR, Samuels AN, Klempner MS, Collins JJ. 2013. *Salmonella typhimurium* intercepts *Escherichia coli* signaling to enhance antibiotic tolerance. Proc Natl Acad Sci U S A 110:14420-5.

9. Hays EE, Wells IC, Katzman PA, Cain CK, Jacobs FA, Thayer SA, Doisy EA, Gaby WL, Roberts EC, Muir RD, Carroll CJ, Jones LR, Wade NJ. 1945. Antibiotic substances produced by *Pseudomonas-aeruginosa*. J Biol Chem 159:725-750.

10. Klumper U, Recker M, Zhang L, Yin X, Zhang T, Buckling A, Gaze WH. 2019. Selection for antimicrobial resistance is reduced when embedded in a natural microbial community. ISME J 13:2927-2937.

11. Liu W, Roder HL, Madsen JS, Bjarnsholt T, Sorensen SJ, Burmolle M. 2016. Interspecific bacterial interactions are reflected in multispecies biofilm spatial organization. Front Microbiol 7:1366.

12. Stacy A, Abraham N, Jorth P, Whiteley M. 2016. Microbial community composition impacts pathogen iron availability during polymicrobial infection. PLoS Pathog 12:e1006084.

13. Rosenthal AZ, Matson EG, Eldar A, Leadbetter JR. 2011. RNA-seq reveals cooperative metabolic interactions between two termite-gut spirochete species in co-culture. ISME J 5:1133-42.

14. Hendrickson EL, Wang T, Dickinson BC, Whitmore SE, Wright CJ, Lamont RJ, Hackett M. 2012. Proteomics of *Streptococcus gordonii* within a model developing oral microbial community. BMC Microbiol 12:211.

15. McKenzie GJ, Harris RS, Lee PL, Rosenberg SM. 2000. The SOS response regulates adaptive mutation. Proc Natl Acad Sci U S A 97:6646-51.

16. Roncarati D, Scarlato V. 2017. Regulation of heat-shock genes in bacteria: from signal sensing to gene expression output. FEMS Microbiol Rev 41:549-574.

17. Amikam D, Galperin MY. 2006. PilZ domain is part of the bacterial c-di-GMP binding protein. Bioinformatics 22:3-6.

18. Keogh D, Tay WH, Ho YY, Dale JL, Chen S, Umashankar S, Williams RBH, Chen SL, Dunny GM, Kline KA. 2016. Enterococcal metabolite cues facilitate interspecies niche modulation and polymicrobial infection. Cell Host Microbe 20:493-503.

19. Lee N, Kim W, Chung J, Lee Y, Cho S, Jang KS, Kim SC, Palsson B, Cho BK. 2020. Iron competition triggers antibiotic biosynthesis in *Streptomyces coelicolor* during coculture with *Myxococcus xanthus*. ISME J 14:1111-1124.

20. Khare A, Tavazoie S. 2015. Multifactorial competition and resistance in a two-species bacterial system. PLoS Genet 11:e1005715.

21. Gjodsbol K, Christensen JJ, Karlsmark T, Jorgensen B, Klein BM, Krogfelt KA. 2006. Multiple bacterial species reside in chronic wounds: a longitudinal study. Int Wound J 3:225-31.

22. Salsgiver EL, Fink AK, Knapp EA, LiPuma JJ, Olivier KN, Marshall BC, Saiman L. 2016. Changing epidemiology of the respiratory bacteriology of patients with cystic fibrosis. Chest 149:390-400.

23. Fischer AJ, Singh SB, LaMarche MM, Maakestad LJ, Kienenberger ZE, Pena TA, Stoltz DA, Limoli DH. 2021. Sustained coinfections with *Staphylococcus aureus* and *Pseudomonas aeruginosa* in cystic fibrosis. Am J Respir Crit Care Med 203:328-338.

24. Serra R, Grande R, Butrico L, Rossi A, Settimio UF, Caroleo B, Amato B, Gallelli L, de Franciscis S. 2015. Chronic wound infections: the role of *Pseudomonas aeruginos*a and *Staphylococcus aureus*. Expert Rev Anti Infect Ther 13:605-13.

25. Maliniak ML, Stecenko AA, McCarty NA. 2016. A longitudinal analysis of chronic MRSA and *Pseudomonas aeruginosa* co-infection in cystic fibrosis: a single-center study. J Cyst Fibros 15:350-6.

26. Cystic Fibrosis Foundation. 2018. Cystic Fibrosis Foundation patient registry 2018 annual data report. Cystic Fibrosis Foundation, Bethesda, MD.,

27. Sagel SD, Gibson RL, Emerson J, McNamara S, Burns JL, Wagener JS, Ramsey BW, Inhaled Tobramycin in Young Children Study G, Cystic Fibrosis Foundation Therapeutics Development N. 2009. Impact of *Pseudomonas* and *Staphylococcus* infection on inflammation and clinical status in young children with cystic fibrosis. J Pediatr 154:183-8.

28. Nguyen AT, Oglesby-Sherrouse AG. 2016. Interactions between *Pseudomonas aeruginosa* and *Staphylococcus aureus* during co-cultivations and polymicrobial infections. Appl Microbiol Biotechnol 100:6141-8.

29. Hotterbeekx A, Kumar-Singh S, Goossens H, Malhotra-Kumar S. 2017. *In vivo* and *in vitro* interactions between *Pseudomonas aeruginosa* and *Staphylococcus* spp. Front Cell Infect Microbiol 7:106.

30. Magalhaes AP, Jorge P, Pereira MO. 2019. *Pseudomonas aeruginosa* and *Staphylococcus aureus* communication in biofilm infections: insights through network and database construction. Crit Rev Microbiol 45:712-728.

31. Yung DBY, Sircombe KJ, Pletzer D. 2021. Friends or enemies? The complicated relationship between *Pseudomonas aeruginosa* and *Staphylococcus aureus*. Mol Microbiol 116:1-15.

32. Nguyen AT, Jones JW, Ruge MA, Kane MA, Oglesby-Sherrouse AG. 2015. Iron depletion enhances production of antimicrobials by *Pseudomonas aeruginosa*. J Bacteriol 197:2265-75.

33. Noto MJ, Burns WJ, Beavers WN, Skaar EP. 2017. Mechanisms of pyocyanin toxicity and genetic determinants of resistance in *Staphylococcus aureus*. J Bacteriol 199.

34. Filkins LM, Graber JA, Olson DG, Dolben EL, Lynd LR, Bhuju S, O'Toole GA. 2015. Coculture of *Staphylococcus aureus with Pseudomonas aeruginosa* drives *S. aureus* towards fermentative metabolism and reduced viability in a cystic fibrosis model. J Bacteriol 197:2252-64.

35. Mashburn LM, Jett AM, Akins DR, Whiteley M. 2005. *Staphylococcus aureus* serves as an iron source for *Pseudomonas aeruginosa* during *in vivo* coculture. J Bacteriol 187:554-66.

36. Korgaonkar AK, Whiteley M. 2011. *Pseudomonas aeruginosa* enhances production of an antimicrobial in response to *N*-acetylglucosamine and peptidoglycan. J Bacteriol 193:909-17.

37. Korgaonkar A, Trivedi U, Rumbaugh KP, Whiteley M. 2013. Community surveillance enhances *Pseudomonas aeruginosa* virulence during polymicrobial infection. Proc Natl Acad Sci U S A 110:1059-64.

38. Yang N, Cao Q, Hu S, Xu C, Fan K, Chen F, Yang CG, Liang H, Wu M, Bae T, Lan L. 2020. Alteration of protein homeostasis mediates the interaction of *Pseudomonas aeruginosa* with *Staphylococcus aureus*. Mol Microbiol 114:423-442.

39. Duan K, Dammel C, Stein J, Rabin H, Surette MG. 2003. Modulation of *Pseudomonas aeruginosa* gene expression by host microflora through interspecies communication. Mol Microbiol 50:1477-91.

40. Rezzonico F, Smits TH, Duffy B. 2012. Detection of AI-2 receptors in genomes of Enterobacteriaceae suggests a role of type-2 quorum sensing in closed ecosystems. Sensors (Basel) 12:6645-65.

41. Limoli DH, Warren EA, Yarrington KD, Donegan NP, Cheung AL, O'Toole GA. 2019. Interspecies interactions induce exploratory motility in *Pseudomonas aeruginosa*. Elife 8.

42. Pallett R, Leslie LJ, Lambert PA, Milic I, Devitt A, Marshall LJ. 2019. Anaerobiosis influences virulence properties of *Pseudomonas aeruginosa* cystic fibrosis isolates and the interaction with *Staphylococcus aureus*. Sci Rep 9:6748.

43. Camus L, Vandenesch F, Moreau K. 2021. From genotype to phenotype: adaptations of *Pseudomonas aeruginosa* to the cystic fibrosis environment. Microb Genom doi:10.1099/mgen.0.000513.

44. Pederick VG, Eijkelkamp BA, Begg SL, Ween MP, McAllister LJ, Paton JC, McDevitt CA. 2015. ZnuA and zinc homeostasis in *Pseudomonas aeruginosa*. Sci Rep 5:13139.

45. Ochsner UA, Vasil ML. 1996. Gene repression by the ferric uptake regulator in *Pseudomonas aeruginosa*: cycle selection of iron-regulated genes. Proc Natl Acad Sci U S A 93:4409-14.

46. Ochsner UA, Wilderman PJ, Vasil AI, Vasil ML. 2002. GeneChip expression analysis of the iron starvation response in *Pseudomonas aeruginosa*: identification of novel pyoverdine biosynthesis genes. Mol Microbiol 45:1277-87.

47. Fey PD, Endres JL, Yajjala VK, Widhelm TJ, Boissy RJ, Bose JL, Bayles KW. 2013. A genetic resource for rapid and comprehensive phenotype screening of nonessential *Staphylococcus aureus* genes. MBio 4:e00537-12.

48. Ghssein G, Brutesco C, Ouerdane L, Fojcik C, Izaute A, Wang S, Hajjar C, Lobinski R, Lemaire D, Richaud P, Voulhoux R, Espaillat A, Cava F, Pignol D, Borezee-Durant E, Arnoux P. 2016. Biosynthesis of a broad-spectrum nicotianamine-like metallophore in *Staphylococcus aureus*. Science 352:1105-9.

49. McFarlane JS, Lamb AL. 2017. Biosynthesis of an opine metallophore by *Pseudomonas aeruginosa*. Biochemistry 56:5967-5971.

50. Grim KP, San Francisco B, Radin JN, Brazel EB, Kelliher JL, Parraga Solorzano PK, Kim PC, McDevitt CA, Kehl-Fie TE. 2017. The metallophore staphylopine enables *Staphylococcus aureus* to compete with the host for zinc and overcome nutritional immunity. mBio 8.

51. Fojcik C, Arnoux P, Ouerdane L, Aigle M, Alfonsi L, Borezee-Durant E. 2018. Independent and cooperative regulation of staphylopine biosynthesis and trafficking by Fur and Zur. Mol Microbiol 108:159-177.

52. Lhospice S, Gomez NO, Ouerdane L, Brutesco C, Ghssein G, Hajjar C, Liratni A, Wang S, Richaud P, Bleves S, Ball G, Borezee-Durant E, Lobinski R, Pignol D, Arnoux P, Voulhoux R. 2017. *Pseudomonas aeruginosa* zinc uptake in chelating environment is primarily mediated by the metallophore pseudopaline. Sci Rep 7:17132.

53. McFarlane JS, Zhang J, Wang S, Lei X, Moran GR, Lamb AL. 2019. Staphylopine and pseudopaline dehydrogenase from bacterial pathogens catalyze reversible reactions and produce stereospecific metallophores. J Biol Chem 294:17988-18001.

54. Zhang J, Zhao T, Yang R, Siridechakorn I, Wang S, Guo Q, Bai Y, Shen HC, Lei X. 2019. De novo synthesis, structural assignment and biological evaluation of pseudopaline, a metallophore produced by *Pseudomonas aeruginosa*. Chem Sci 10:6635-6641.

55. Gomez NO, Tetard A, Ouerdane L, Laffont C, Brutesco C, Ball G, Lobinski R, Denis Y, Plesiat P, Llanes C, Arnoux P, Voulhoux R. 2020. Involvement of the *Pseudomonas aeruginosa* MexAB-OprM efflux pump in the secretion of the metallophore pseudopaline. Mol Microbiol doi:10.1111/mmi.14600.

56. Furman R, Biswas T, Danhart EM, Foster MP, Tsodikov OV, Artsimovitch I. 2013. DksA2, a zinc-independent structural analog of the transcription factor DksA. FEBS Lett 587:614-9.

57. Wakeman CA, Moore JL, Noto MJ, Zhang Y, Singleton MD, Prentice BM, Gilston BA, Doster RS, Gaddy JA, Chazin WJ, Caprioli RM, Skaar EP. 2016. The innate immune protein calprotectin promotes *Pseudomonas aeruginosa* and *Staphylococcus aureus* interaction. Nat Commun 7:11951.

58. Vermilyea DM, Crocker AW, Gifford AH, Hogan DA. 2021. Calprotectin-mediated zinc chelation inhibits *Pseudomonas aeruginosa* protease activity in cystic fibrosis sputum. J Bacteriol 203:e0010021.

59. Marguerettaz M, Dieppois G, Que YA, Ducret V, Zuchuat S, Perron K. 2014. Sputum containing zinc enhances carbapenem resistance, biofilm formation and virulence of *Pseudomonas aeruginosa*. Microb Pathog 77:36-41.

60. Banin E, Vasil ML, Greenberg EP. 2005. Iron and *Pseudomonas aeruginosa* biofilm formation. Proc Natl Acad Sci U S A 102:11076-81.

61. Cuiv PO, Keogh D, Clarke P, O'Connell M. 2007. FoxB of *Pseudomonas aeruginosa* functions in the utilization of the xenosiderophores ferrichrome, ferrioxamine B, and schizokinen: evidence for transport redundancy at the inner membrane. J Bacteriol 189:284-7.

62. O'May CY, Sanderson K, Roddam LF, Kirov SM, Reid DW. 2009. Iron-binding compounds impair *Pseudomonas aeruginosa* biofilm formation, especially under anaerobic conditions. J Med Microbiol 58:765-773.

63. Visca P, Bonchi C, Minandri F, Frangipani E, Imperi F. 2013. The dual personality of iron chelators: growth inhibitors or promoters? Antimicrob Agents Chemother 57:2432-3.

64. Tamber S, Maier E, Benz R, Hancock RE. 2007. Characterization of OpdH, a *Pseudomonas aeruginosa* porin involved in the uptake of tricarboxylates. J Bacteriol 189:929-39.

65. Ashburner M, Ball CA, Blake JA, Botstein D, Butler H, Cherry JM, Davis AP, Dolinski K, Dwight SS, Eppig JT, Harris MA, Hill DP, Issel-Tarver L, Kasarskis A, Lewis S, Matese JC, Richardson JE, Ringwald M, Rubin GM, Sherlock G. 2000. Gene ontology: tool for the unification of biology. The Gene Ontology Consortium. Nat Genet 25:25-9.

66. Mi H, Muruganujan A, Ebert D, Huang X, Thomas PD. 2019. PANTHER version 14: more genomes, a new PANTHER GO-slim and improvements in enrichment analysis tools. Nucleic Acids Res 47:D419-D426.

67. Gene Ontology C. 2021. The Gene Ontology resource: enriching a GOld mine. Nucleic Acids Res 49:D325-D334.

68. Xiao Z, Xu P. 2007. Acetoin metabolism in bacteria. Crit Rev Microbiol 33:127-40.

69. Liu Q, Liu Y, Kang Z, Xiao D, Gao C, Xu P, Ma C. 2018. 2,3-Butanediol catabolism in *Pseudomonas aeruginosa* PAO1. Environ Microbiol 20:3927-3940.

70. Camus L, Briaud P, Bastien S, Elsen S, Doleans-Jordheim A, Vandenesch F, Moreau K. 2020. Trophic cooperation promotes bacterial survival of *Staphylococcus aureus and Pseudomonas aeruginosa*. ISME J 14:3093-3105.

71. Blanusa M, Varnai VM, Piasek M, Kostial K. 2005. Chelators as antidotes of metal toxicity: therapeutic and experimental aspects. Curr Med Chem 12:2771-94.

72. Mastropasqua MC, Lamont I, Martin LW, Reid DW, D'Orazio M, Battistoni A. 2018. Efficient zinc uptake is critical for the ability of *Pseudomonas aeruginosa* to express virulence traits and colonize the human lung. J Trace Elem Med Biol 48:74-80.

73. Gray RD, Duncan A, Noble D, Imrie M, O'Reilly DS, Innes JA, Porteous DJ, Greening AP, Boyd AC. 2010. Sputum trace metals are biomarkers of inflammatory and suppurative lung disease. Chest 137:635-41.

74. Gonzalez MR, Ducret V, Leoni S, Perron K. 2019. *Pseudomonas aeruginosa* zinc homeostasis: Key issues for an opportunistic pathogen. Biochim Biophys Acta Gene Regul Mech 1862:722-733.

75. Conrady DG, Brescia CC, Horii K, Weiss AA, Hassett DJ, Herr AB. 2008. A zinc-dependent adhesion module is responsible for intercellular adhesion in staphylococcal biofilms. Proc Natl Acad Sci U S A 105:19456-61.

76. Ding Y, Fu Y, Lee JC, Hooper DC. 2012. *Staphylococcus aureus* NorD, a putative efflux pump coregulated with the Opp1 oligopeptide permease, contributes selectively to fitness *in vivo*. J Bacteriol 194:6586-93.

77. Formosa-Dague C, Speziale P, Foster TJ, Geoghegan JA, Dufrene YF. 2016. Zinc-dependent mechanical properties of *Staphylococcus aureus* biofilm-forming surface protein SasG. Proc Natl Acad Sci U S A 113:410-5.

78. Li K, Gifford AH, Hampton TH, O'Toole GA. 2020. Availability of zinc impacts interactions between *Streptococcus sanguinis* and *Pseudomonas aeruginosa* in coculture. J Bacteriol 202.

79. Rossi E, Falcone M, Molin S, Johansen HK. 2018. High-resolution in situ transcriptomics of *Pseudomonas aeruginosa* unveils genotype independent patho-phenotypes in cystic fibrosis lungs. Nat Commun 9:3459.

80. Cornforth DM, Dees JL, Ibberson CB, Huse HK, Mathiesen IH, Kirketerp-Moller K, Wolcott RD, Rumbaugh KP, Bjarnsholt T, Whiteley M. 2018. *Pseudomonas aeruginosa* transcriptome during human infection. Proc Natl Acad Sci U S A 115:E5125-E5134.

81. Kordes A, Preusse M, Willger SD, Braubach P, Jonigk D, Haverich A, Warnecke G, Haussler S. 2019. Genetically diverse *Pseudomonas aeruginosa* populations display similar transcriptomic profiles in a cystic fibrosis explanted lung. Nat Commun 10:3397.

82. Harrison F, Paul J, Massey RC, Buckling A. 2008. Interspecific competition and siderophore-mediated cooperation in *Pseudomonas aeruginosa*. ISME J 2:49-55.

83. Tognon M, Kohler T, Luscher A, van Delden C. 2019. Transcriptional profiling of *Pseudomonas aeruginosa* and *Staphylococcus aureus* during *in vitro* co-culture. BMC Genomics 20:30.

84. Barber MF, Elde NC. 2015. Buried treasure: evolutionary perspectives on microbial iron piracy. Trends Genet 31:627-636.

85. Farrand AJ, Reniere ML, Ingmer H, Frees D, Skaar EP. 2013. Regulation of host hemoglobin binding by the *Staphylococcus aureus* Clp proteolytic system. J Bacteriol 195:5041-50.

86. Farrand AJ, Friedman DB, Reniere ML, Ingmer H, Frees D, Skaar EP. 2015. Proteomic analyses of iron-responsive, Clp-dependent changes in *Staphylococcus aureus*. Pathog Dis 73.

87. Pacheco AR, Moel M, Segre D. 2019. Costless metabolic secretions as drivers of interspecies interactions in microbial ecosystems. Nat Commun 10:103.

88. Taylor PK, Zhang L, Mah TF. 2019. Loss of the two-component system TctD-TctE in *Pseudomonas aeruginosa* affects biofilm formation and aminoglycoside susceptibility in response to citric acid. mSphere 4.

89. Dunphy LJ, Yen P, Papin JA. 2019. Integrated experimental and computational analyses reveal differential metabolic functionality in antibiotic-resistant *Pseudomonas aeruginosa*. Cell Syst 8:3-14 e3.

90. Dunphy LJ, Grimes KL, Wase N, Kolling GL, Papin JA. 2021. Untargeted metabolomics reveals species-specific metabolite production and shared nutrient consumption by *Pseudomonas aeruginosa* and *Staphylococcus aureus*. mSystems 6:e0048021.

971 91. Carvalho SM, de Jong A, Kloosterman TG, Kuipers OP, Saraiva LM. 2017. The
972 *Staphylococcus aureus* alpha-acetolactate synthase ALS confers resistance to
973 nitrosative stress. Front Microbiol 8:1273.

974 92. Mould DL, Botelho NJ, Hogan DA. 2020. Intraspecies signaling between common
975 variants of *Pseudomonas aeruginosa* increases production of quorum-sensing-controlled
976 virulence factors. mBio 11.

977 93. Marshall B, Stintzi A, Gilmour C, Meyer JM, Poole K. 2009. Citrate-mediated iron uptake
978 in *Pseudomonas aeruginosa*: involvement of the citrate-inducible FecA receptor and the
979 FeoB ferrous iron transporter. Microbiology (Reading) 155:305-315.

980 94. Ding Y, Liu X, Chen F, Di H, Xu B, Zhou L, Deng X, Wu M, Yang CG, Lan L. 2014.
981 Metabolic sensor governing bacterial virulence in *Staphylococcus aureus*. Proc Natl
982 Acad Sci U S A 111:E4981-90.

983 95. Li H, Li X, Wang Z, Fu Y, Ai Q, Dong Y, Yu J. 2015. Autoinducer-2 regulates
984 *Pseudomonas aeruginosa* PAO1 biofilm formation and virulence production in a dose-
985 dependent manner. BMC Microbiol 15:192.

986 96. Peters JM, Koo BM, Patino R, Heussler GE, Hearne CC, Qu J, Inclan YF, Hawkins JS,
987 Lu CHS, Silvis MR, Harden MM, Osadnik H, Peters JE, Engel JN, Dutton RJ, Grossman
988 AD, Gross CA, Rosenberg OS. 2019. Enabling genetic analysis of diverse bacteria with
989 Mobile-CRISPRi. Nat Microbiol 4:244-250.

990 97. Jiang W, Oikonomou P, Tavazoie S. 2020. Comprehensive genome-wide perturbations
991 via CRISPR adaptation reveal complex genetics of antibiotic sensitivity. Cell 180:1002-
992 1017 e31.

993 98. Shiver AL, Culver R, Deutschbauer AM, Huang KC. 2021. Rapid ordering of barcoded
994 transposon insertion libraries of anaerobic bacteria. Nat Protoc 16:3049-3071.

995 99. Rahme LG, Stevens EJ, Wolfort SF, Shao J, Tompkins RG, Ausubel FM. 1995.
996 Common virulence factors for bacterial pathogenicity in plants and animals. Science
997 268:1899-902.

998 100. Pardee AB, Jacob F, Monod J. 1959. Genetic control and cytoplasmic expression of
999 inducibility in the synthesis of beta-galactosidase by *E-coli*. J Mol Biol 1:165-178.

1000 101. Martin M. 2011. Cutadapt removes adapter sequences from high-throughput sequencing
1001 reads. EMBnet J 17:10-12.

1002 102. Bolger AM, Lohse M, Usadel B. 2014. Trimmomatic: a flexible trimmer for Illumina
1003 sequence data. Bioinformatics 30:2114-20.

1004 103. McClure R, Balasubramanian D, Sun Y, Bobrovskyy M, Sumby P, Genco CA,
1005 Vanderpool CK, Tjaden B. 2013. Computational analysis of bacterial RNA-Seq data.
1006 Nucleic Acids Res 41:e140.

1007 104. Tjaden B. 2015. *De novo* assembly of bacterial transcriptomes from RNA-seq data.
1008 Genome Biol 16:1.

105. Tretyakov K. 2020. matplotlib_venn, GitHub repository.

106. Krassowski M. 2020. ComplexUpset doi:10.5281/zenodo.3700590.

107. Wang B, Lin YC, Vasquez-Rifo A, Jo J, Price-Whelan A, McDonald ST, Brown LM, Sieben C, Dietrich LEP. 2021. *Pseudomonas aeruginosa* PA14 produces R-bodies, extendable protein polymers with roles in host colonization and virulence. Nat Commun 12:4613.

108. Hoang TT, Karkhoff-Schweizer RR, Kutchma AJ, Schweizer HP. 1998. A broad-host-range Flp-FRT recombination system for site-specific excision of chromosomally-located DNA sequences: application for isolation of unmarked *Pseudomonas aeruginosa* mutants. Gene 212:77-86.

109. Elliott RP. 1958. Some properties of pyoverdine, the water-soluble fluorescent pigment of the pseudomonads. Appl Microbiol 6:241-6.

110. Winsor GL, Griffiths EJ, Lo R, Dhillon BK, Shay JA, Brinkman FS. 2016. Enhanced annotations and features for comparing thousands of *Pseudomonas genomes* in the *Pseudomonas* genome database. Nucleic Acids Res 44:D646-53.

111. Fuchs S, Mehlan H, Bernhardt J, Hennig A, Michalik S, Surmann K, Pane-Farre J, Giese A, Weiss S, Backert L, Herbig A, Nieselt K, Hecker M, Volker U, Mader U. 2018. AureoWiki The repository of the *Staphylococcus aureus* research and annotation community. Int J Med Microbiol 308:558-568.

112. O'Toole GA. 2011. Microtiter dish biofilm formation assay. J Vis Exp doi:10.3791/2437.

113. Himpsl SDM, E.L.T. 2019. Siderophore detection using chrome azurol S and cross-feeding assays. *In* Pearson M (ed), *Proteus mirabilis*: Methods in Molecular Biology, vol vol 2021. Humana, New York, NY.

114. Nicholson WL. 2008. The *Bacillus subtilis ydjL* (*bdhA*) gene encodes acetoin reductase/2,3-butanediol dehydrogenase. Appl Environ Microbiol 74:6832-8.

115. Dorau R, Chen L, Liu J, Jensen PR, Solem C. 2019. Efficient production of alpha-acetolactate by whole cell catalytic transformation of fermentation-derived pyruvate. Microb Cell Fact 18:217.

116. Chen J, Chen D, Zhang X, Wang M, Chen B, An D, Xu L, Lyu Q. 2018. Quantification of alcohols, diols and glycerol in fermentation with an instantaneous derivatization using trichloroacetyl isocyanante via liquid chromatography-massspectrometry. J Chromatogr A 1568:22-28.

FIGURES AND FIGURE LEGENDS

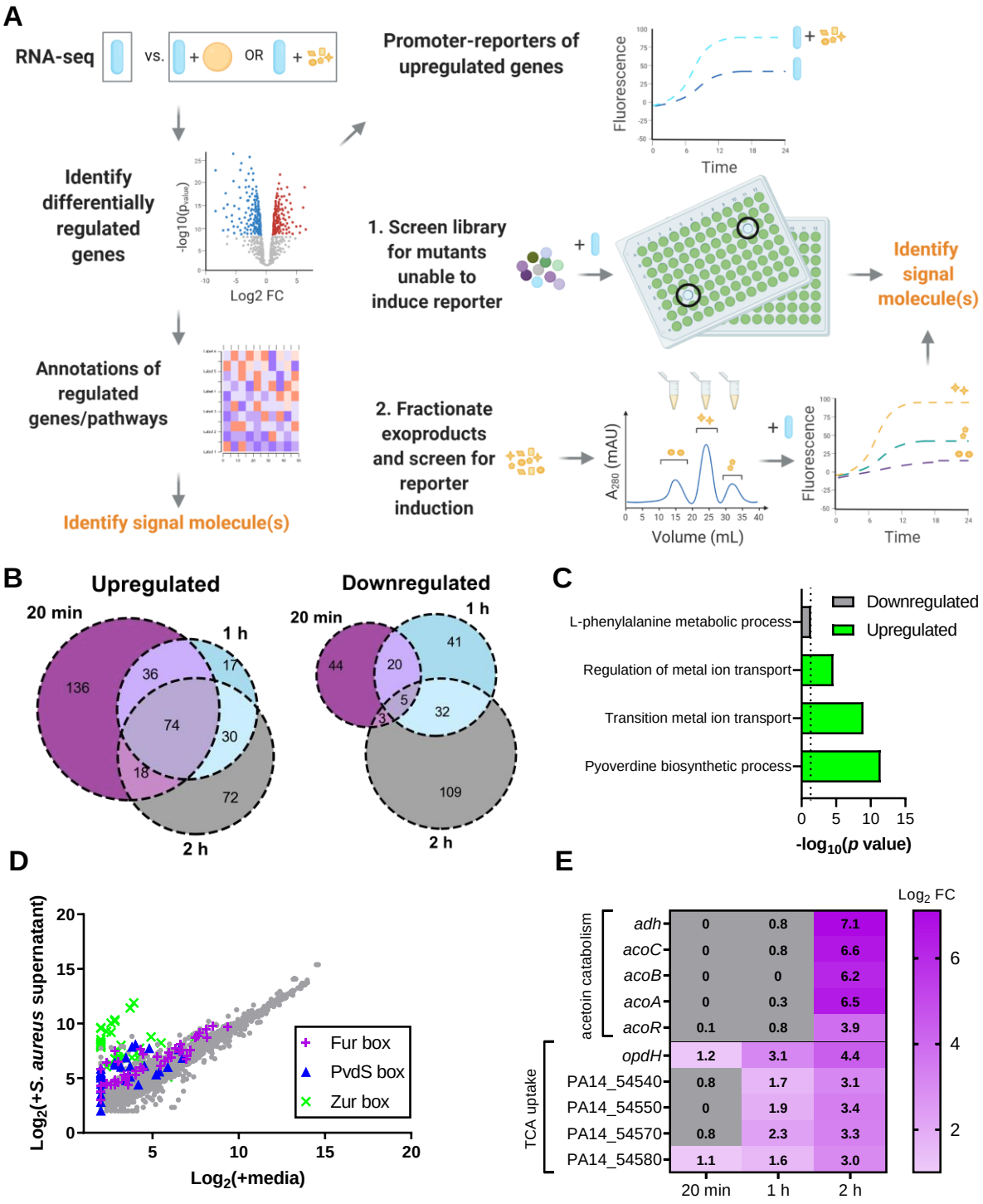

FIGURE 1. *P. aeruginosa* differentially regulates metal deprivation and intermediate metabolite uptake pathways in the presence of *S. aureus* supernatant. (A) Schematic for

identification of molecular mediators of interspecies sensing in a two-species system. Global transcriptional response of one species to another species, or its secreted exoproducts, compared to monocultures, is determined by RNA-seq. Analysis of the differentially regulated genes and pathways may be used to identify the signaling molecules that are sensed. Promoter-reporters are constructed from representative upregulated genes and used to screen for the signaling molecules by two complementary methods. In the first method, a mutant library is screened for mutants that disrupt production or export of the signaling molecules, and therefore have lower reporter expression. In the second, the supernatant is biochemically fractionated and fractions are screened for induction of the promoter. **(B)** Venn diagrams of upregulated and downregulated genes (Log_2 fold change ≥ 1 or ≤ -1 and $p < 0.05$ cutoff) in *P. aeruginosa* after *S. aureus* supernatant exposure compared to media control after 20 min, 1 h, and 2 h. **(C)** Gene ontology (GO) enrichment of differentially expressed genes in *P. aeruginosa* after 20 min (2). Non-redundant categories for downregulated and upregulated biological processes are shown. **(D)** Scatterplot of mean expression levels of transcripts after *S. aureus* supernatant exposure compared to media control after 20 min. Genes annotated previously in *P. aeruginosa* strain PAO1 as being regulated by Fur, PvdS (IS box), or Zur are shown (3, 4). **(E)** Log_2 fold change of select transcripts in metabolite-uptake operons that increase in abundance over time.

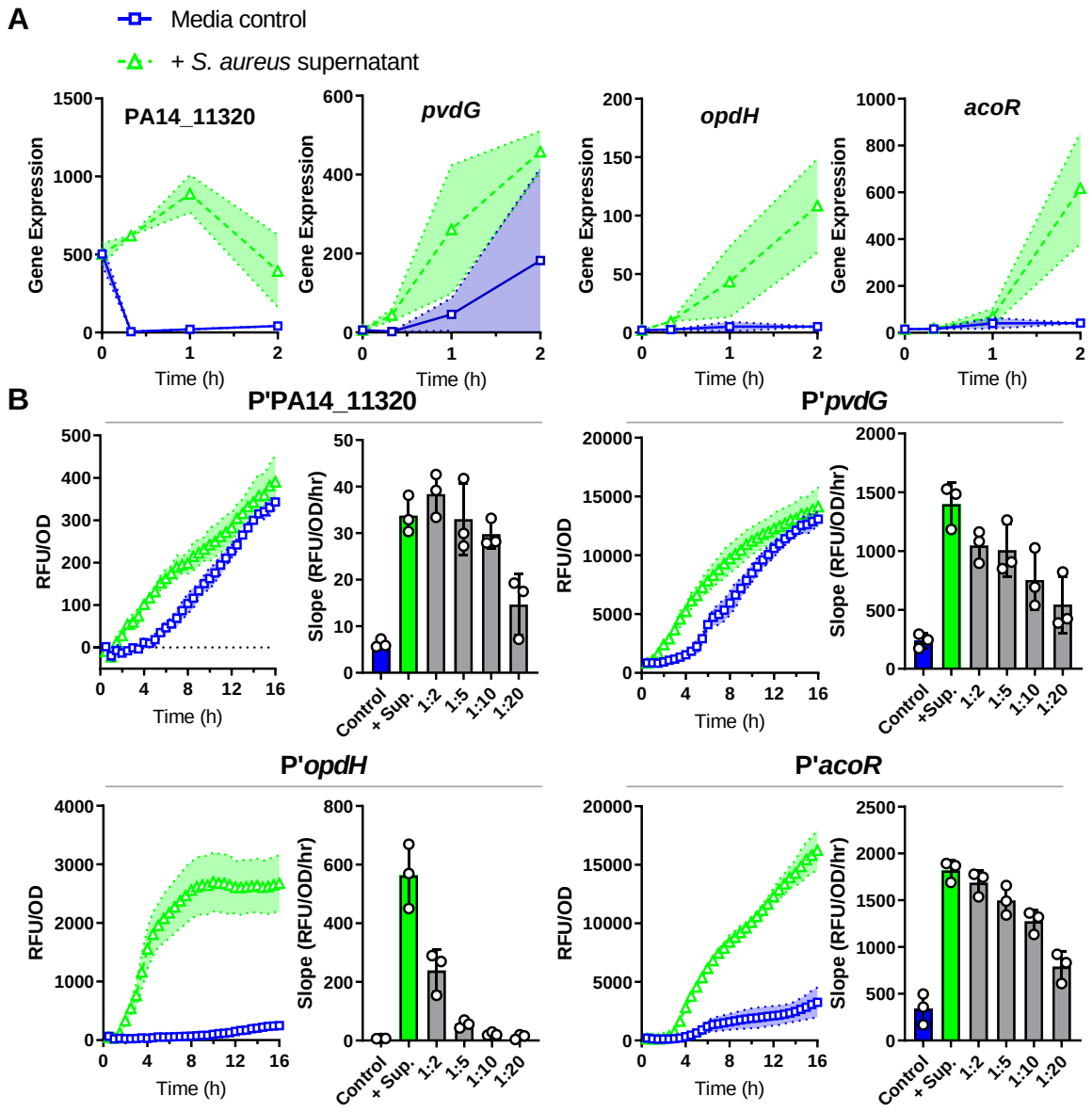

FIGURE 2. *P. aeruginosa* promoter-reporters are induced by *S. aureus* exoproducts. (A) Expression levels from RNA-seq after exposure to *S. aureus* supernatant or media control for four transcripts as gene candidates for promoter-reporter construction. Gene annotations: PA14_11320, Zur-regulon putative lipoprotein in operon with ABC transporter; *pvdG*, pyoverdine biosynthesis thioesterase; *opdH*, TCA uptake porin; *acoR*, transcriptional regulator of acetoin catabolism genes. **(B)** Relative fluorescence units (RFU) of mScarlet normalized to OD_{600} over time after exposure to *S. aureus* supernatant or media control in the indicated promoter-reporter

1071 strains. Slope calculated from 1.5-5 h (promoters of PA14_11320, *opdH*, and *acoR*) or 1-4 h
1072 (promoter of *pvdG*) after addition of supernatant, supernatant dilutions, or media control. Each
1073 strain had higher expression of mScarlet after supernatant addition compared with media control
1074 and displayed dose-dependent responses. Shaded regions and error bars show the standard
1075 deviation (SD).

1076

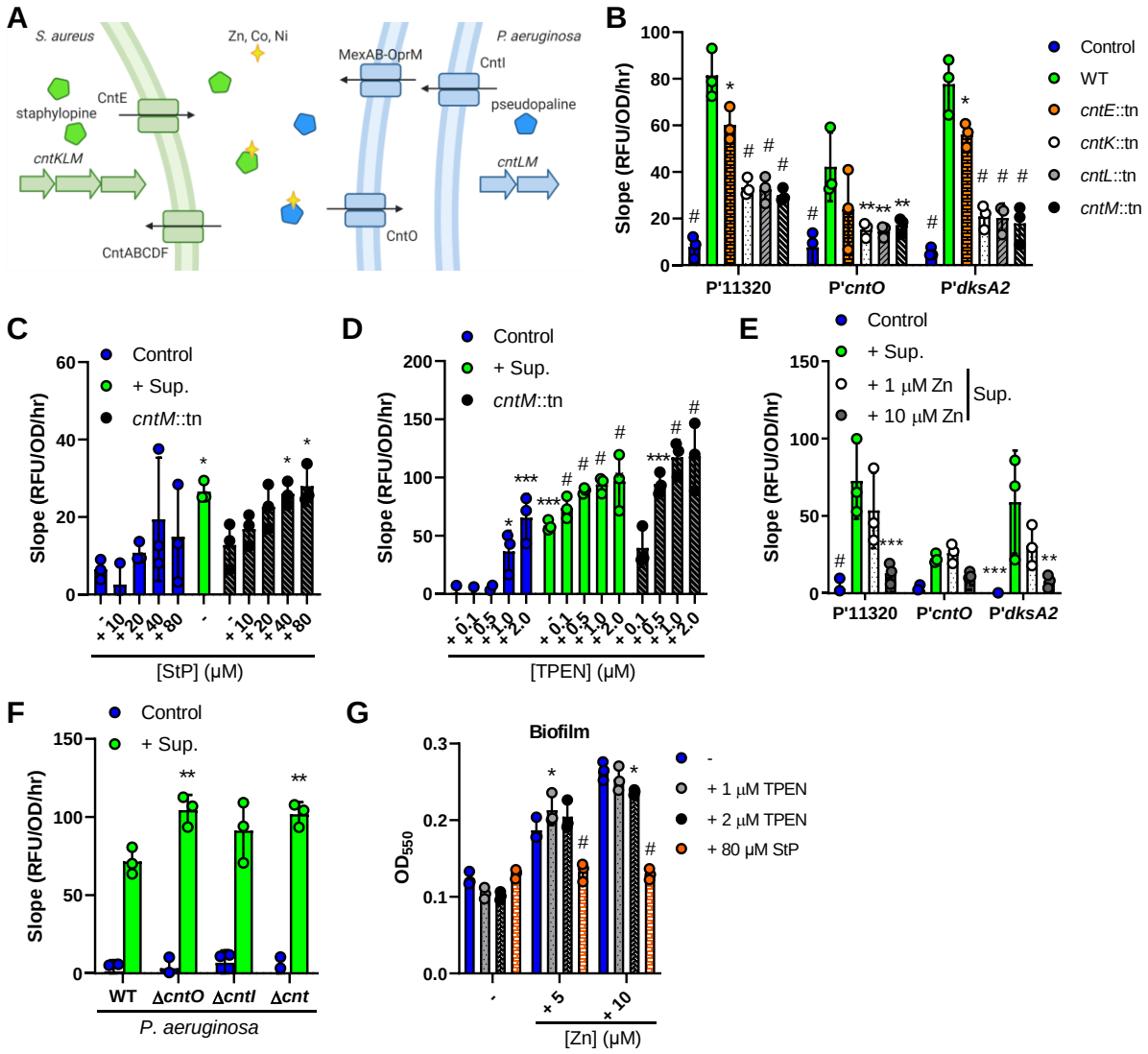

1077

1078 **FIGURE 3. The *S. aureus* metallophore staphylopine is sensed by *P. aeruginosa*. (A)**
1079 Screening of the NTML identified mutants in the biosynthesis and secretion of staphylopine (StP)
1080 as deficient in the induction of the PA14_11320 promoter. Schematic shows StP (green pentagon)
1081 and pseudopaline (PsP) (blue pentagon) biosynthesis, export, binding to transition metals Zn, Co,
1082 Ni, and uptake. **(B-F)** RFU of mScarlet normalized to OD_{600} over time from 1.5 to 5 h after
1083 exposure to media control or *S. aureus* WT or *cnt* supernatant and/or addition of the indicated
1084 concentrations of StP, Zn, or TPEN in the indicated *P. aeruginosa* WT or mutant promoter-

reporter strains. **(G)** *P. aeruginosa* cultures were grown in medium alone or with the additives listed, and biofilm formation was assessed by crystal violet staining after 24 h of growth. Data shown for all panels are the means of three independent biological replicates. Datasets were analyzed by two-way ANOVA with Tukey's test for multiple comparisons (significance shown for comparisons to: B, WT supernatant; F, respective WT sample, respectively) or one-way ANOVA with Dunnett's test for multiple comparisons to the respective control (E, WT supernatant; C, D, and G, media control). The error bars denote the SD. *, p <0.05; **, p <0.01; ***, p <0.001; #, p <0.0001.

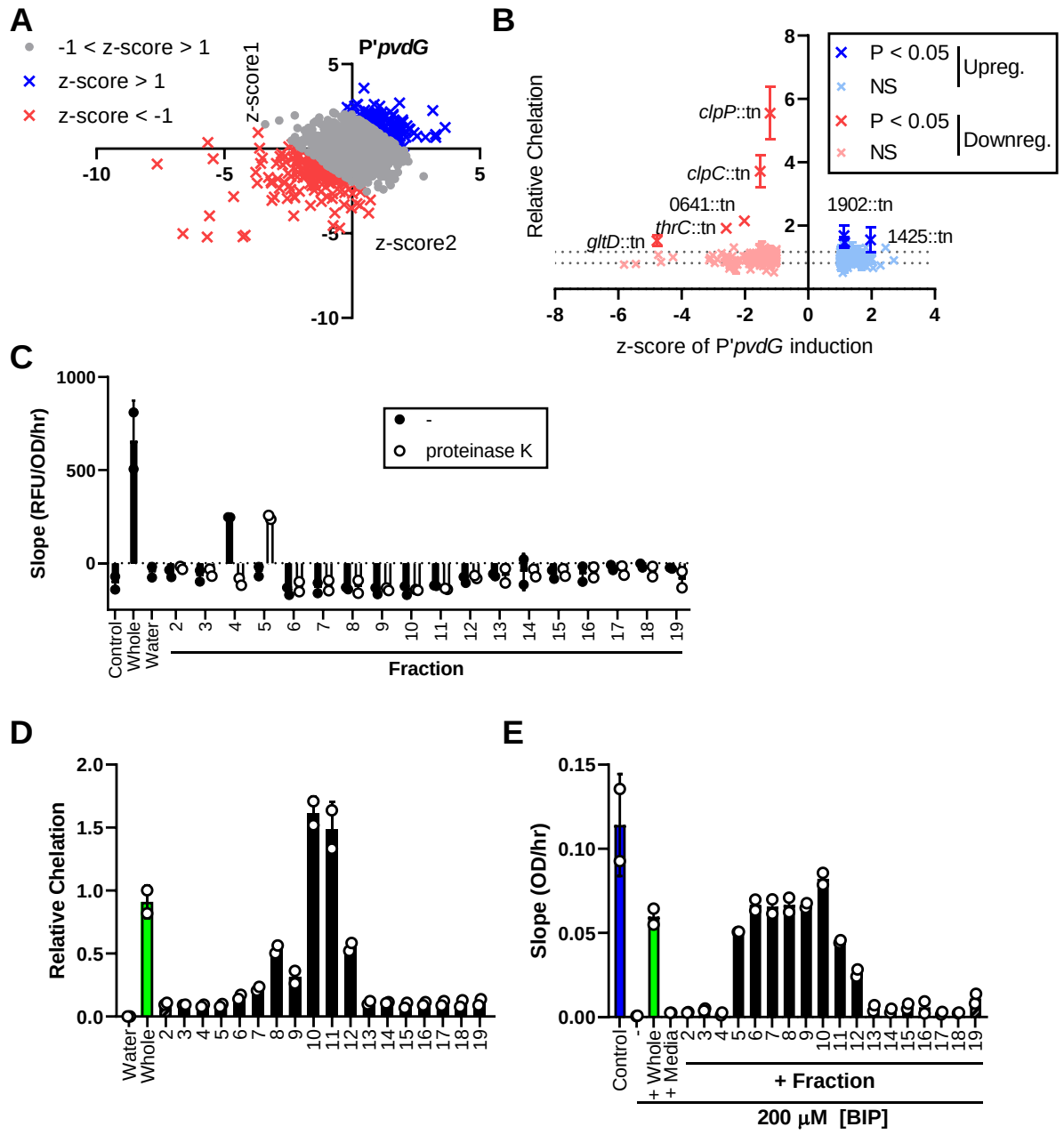

FIGURE 4. *P. aeruginosa* pyoverdine promoter induction is affected by multiple *S. aureus* secreted factors. (A) Transposon library screen with P'*pvdG*-reporter strain to determine mutations in *S. aureus* that increase or decrease induction in *P. aeruginosa*. For each mutant supernatant, the z-scores calculated from the mean slope (RFU/OD_{600}/hr) of each respective experiment for two replicates of the screen are shown. (z-score < -1, downregulating, red; z-score

> 1, upregulating, blue). **(B)** Relative chelation of the downregulating and upregulating supernatants (r = -0.04 for correlation between the relative chelation and the z-score). Data was analyzed by one-way ANOVA with Dunnett's test for multiple comparisons to the WT control. Supernatants with significantly different chelation compared to the WT control are labeled. Data shown represent three independent replicates. **(C-E)** WT *S. aureus* supernatant was fractionated by size-exclusion chromatography. Two independent biological replicates are shown. **(C)** RFU of mScarlet normalized to OD_{600} over time from 1 to 4 h after exposure to media control, 1X whole *S. aureus* WT supernatant, water, or 10X fractions with or without proteinase K treatment (mixed 1:1 with medium). **(D)** Relative chelation of water control, whole supernatant, or 10X fractions. **(E)** Slope of OD_{600} over time from 1 to 8 h of *P. aeruginosa* Δ*pvdJ* Δ*pchE* strain in medium control or medium with 200 µM BIP with the addition of whole WT *S. aureus* supernatant, media, or 10X fractions. Error bars denote the SD for panels B-E.

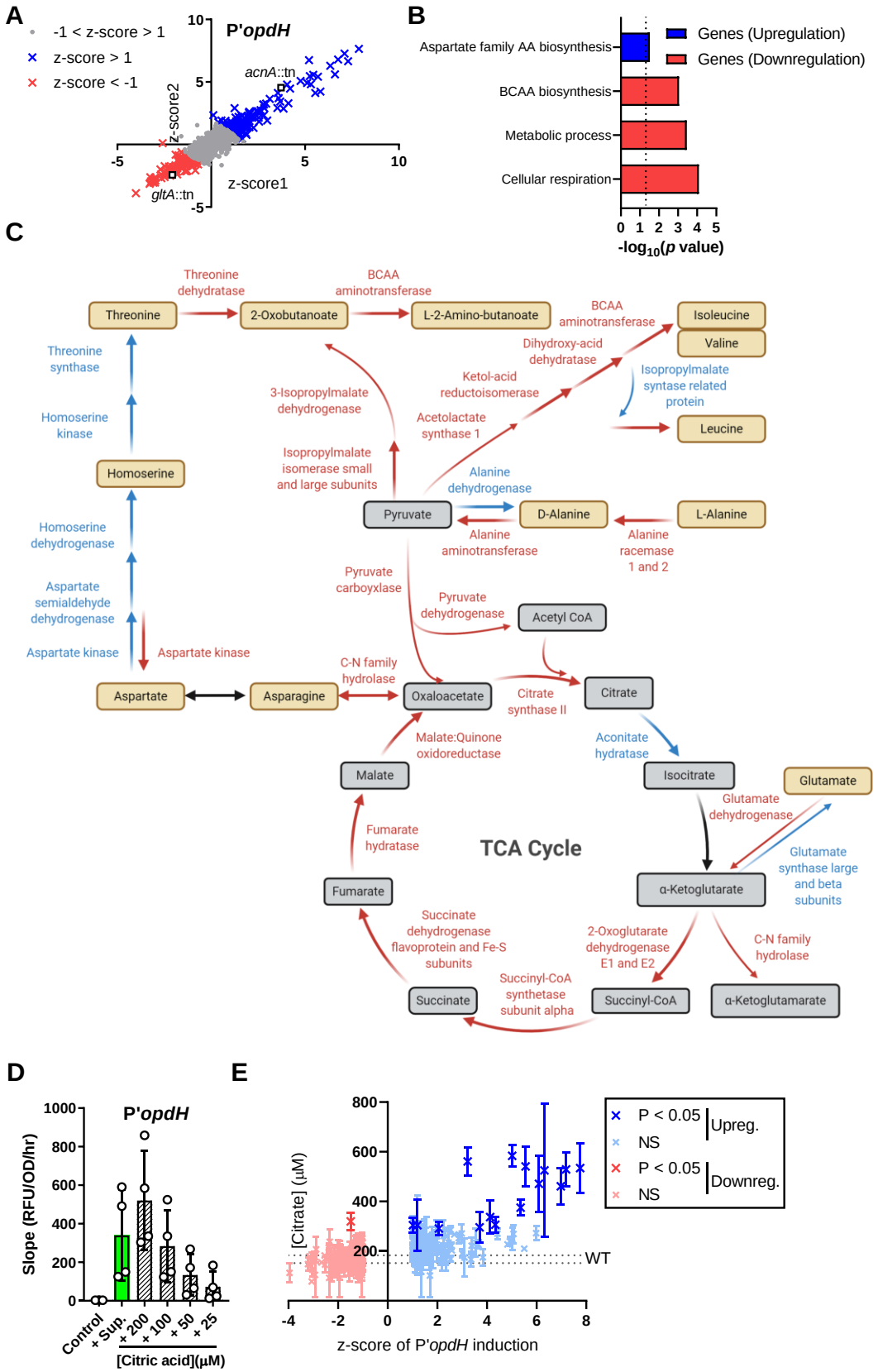

1111

FIGURE 5. *S. aureus*-secreted citrate is sensed by *P. aeruginosa*. (A) Transposon library screen with P'*opdH*-reporter strain to determine mutations in *S. aureus* that increase or decrease induction in *P. aeruginosa*. For each mutant supernatant, the z-scores calculated from the mean slope (RFU/OD_{600}/hr) of each respective experiment for two replicates of the screen are shown (z-score < -1, downregulating, red; z-score > 1, upregulating, blue). **(B)** GO enrichment analysis of downregulating and upregulating mutants. **(C)** Enzymatic reactions in central metabolism are shown, with the colors representing the effect of the mutant supernatants on promoter induction (downregulating, red; upregulating, blue; mutant not in library and/or no change, black). **(D)** RFU of P'*opdH*-mScarlet normalized to OD_{600} over time from 1.5 to 5 h after exposure to media control, *S. aureus* supernatant, or dilutions of citric acid. **(E)** Citric acid measurements of the downregulating and upregulating supernatants correlate to their induction of the P'*opdH* promoter (r = 0.6663). Data was analyzed by one-way ANOVA with Dunnett's test for multiple comparisons to the WT control. Data shown represent three independent replicates for panels D-E. Error bars denote the SD for panels D-E.

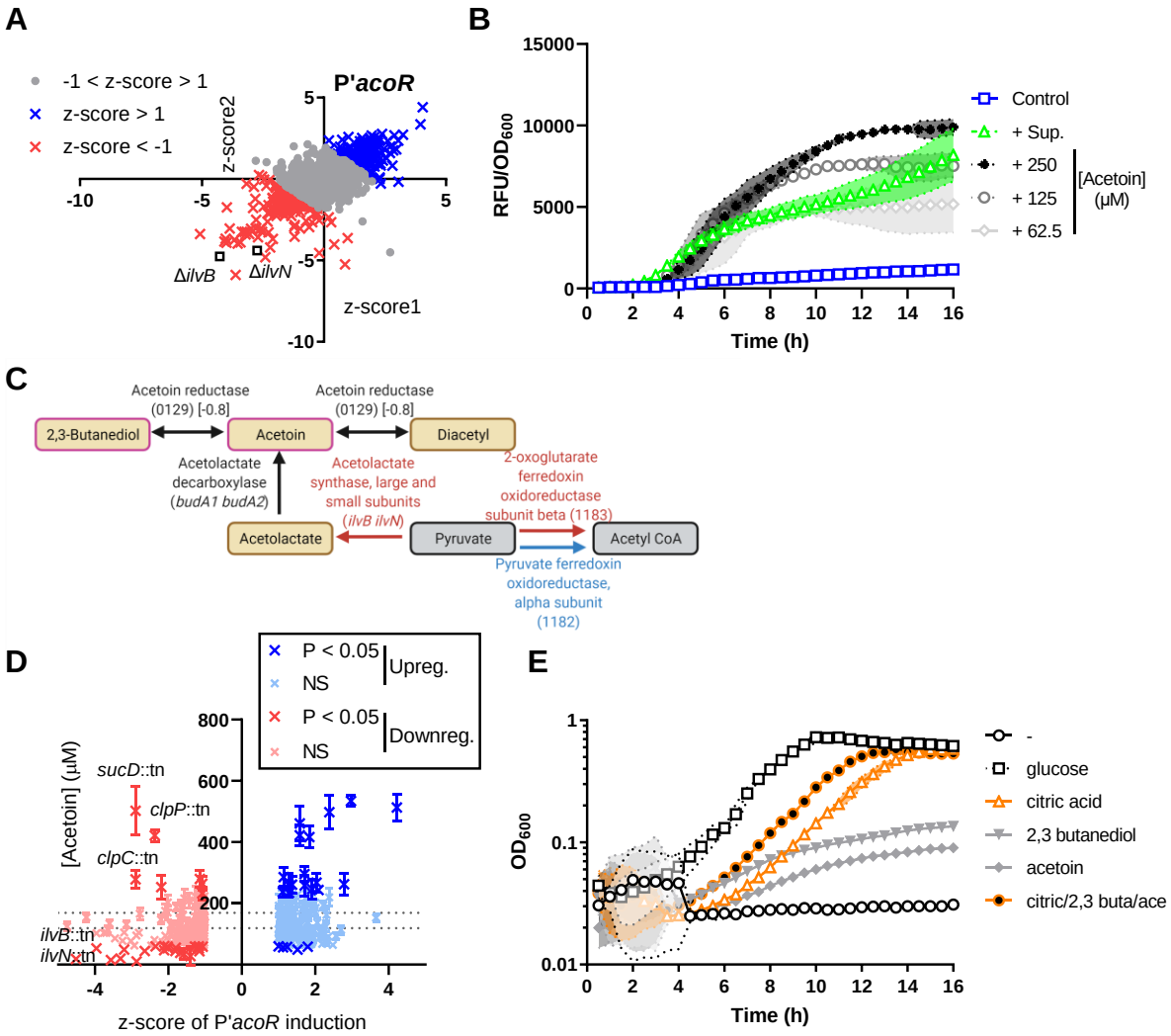

FIGURE 6. Intermediate metabolites produced by *S. aureus* are sensed and utilized as carbon sources by *P. aeruginosa*. (A) Transposon library screen with P'*acoR*-reporter strain to determine mutations in *S. aureus* that increase or decrease induction in *P. aeruginosa*. For each mutant supernatant, the z-scores calculated from the mean slope (RFU/OD_{600}/hr) of each respective experiment for two replicates of the screen are shown (z-score < -1, downregulating, red; z-score > 1, upregulating, blue). **(B)** RFU per OD_{600} of P'*acoR*-mScarlet after addition of media, *S. aureus* supernatant, or the indicated concentrations of acetoin. **(C)** Enzymatic reactions of butanoate metabolism are shown, with the colors representing the effect of the mutant

supernatants on promoter induction (downregulating, red; upregulating, blue; mutant not in library and/or no change, black). **(D)** Acetoin measurements of the upregulating and downregulating supernatants correlate with P'*acoR* induction (r = 0.2157). Acetoin concentration data was analyzed by one-way ANOVA with Dunnett's test for multiple comparisons to the WT control. For panels B and D, data shown represent three independent replicates and error bars denote the SD. **(E)** Growth of *P. aeruginosa* was monitored at OD_{600} after the addition of 1 mM glucose, citric acid, 2,3-butanediol, acetoin, or a mix of citric acid, 2,3-butanediol, and acetoin as the sole carbon sources. Two independent replicates are shown. Shaded regions denote the SD.

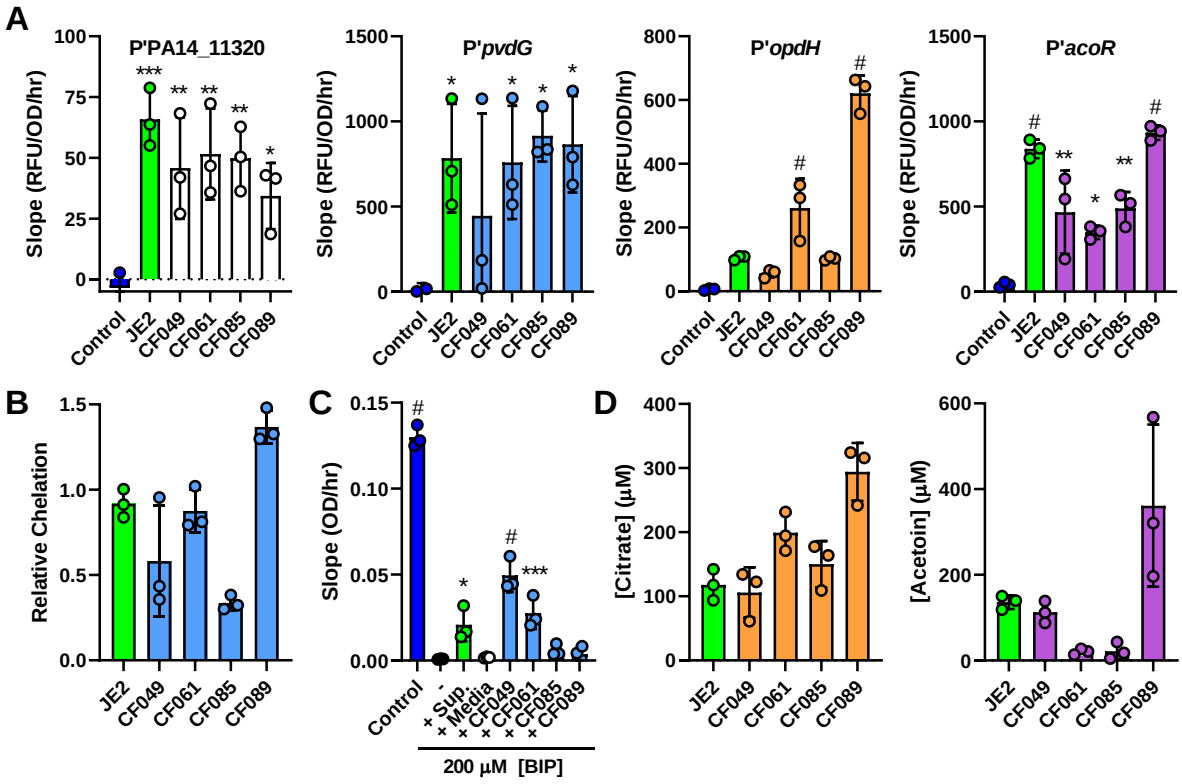

FIGURE 7. Sensed exoproducts are secreted by *S. aureus* clinical isolates. (A) RFU of mScarlet normalized to OD_{600} over time (promoter of PA14_11320, *opdH*, and *acoR* calculated from 1.5 to 5 h; promoter of *pvdG* calculated from 1 to 4 h) of the indicated promoter-reporter strains after exposure to media control, or supernatants from *S. aureus* JE2 or clinical isolates CF049, CF061, CF085, and CF089. **(B)** Relative chelation of supernatants collected from *S. aureus* JE2 or the indicated clinical isolate. **(C)** Slope of OD_{600} over time from 1 to 8 h of *P. aeruginosa* Δ*pvdJ* Δ*pchE* strain in medium control or medium with 200 µM BIP with the addition of medium or supernatant from *S. aureus* JE2 or the indicated clinical isolate. **(D)** Citrate and acetoin measurements of supernatants collected from *S. aureus* JE2 or the indicated clinical isolates. For panels A and C, datasets were analyzed by one-way ANOVA with Dunnett's test for multiple comparisons to the media only control for A and no addition for C. Three independent

1157 replicates shown for all panels. Error bars denote the SD. *, p <0.05; **, p <0.01; ***, p <0.001; #,

1158 p <0.0001.

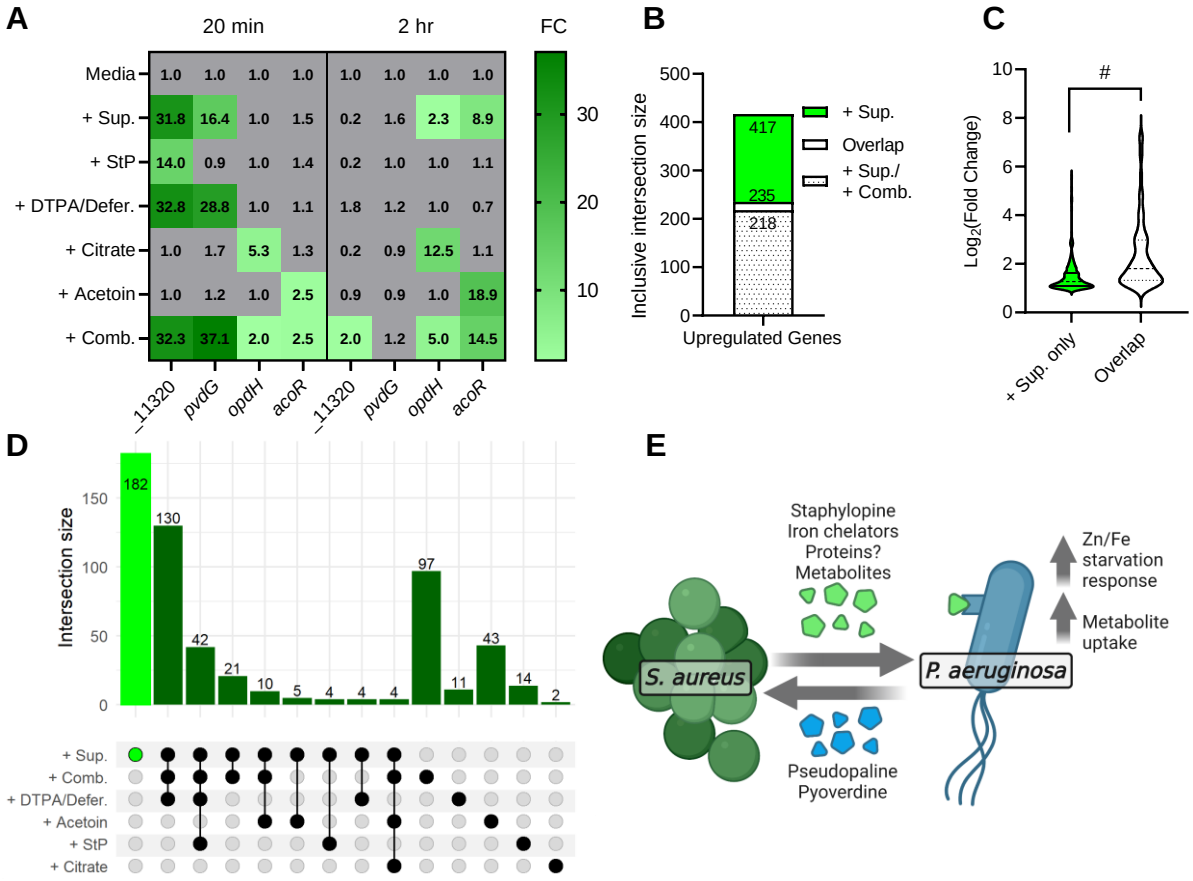

FIGURE 8. Identified sensed products recapitulate a major part of the *P. aeruginosa* response to *S. aureus* supernatant. (A) Heatmap of fold change of the transcripts PA14_11320, *pvdG*, *opdH*, and *acoR* after addition of *S. aureus* supernatant, the indicated molecules, or all molecules in combination (+ Comb.) over media control, after 20 min or 2 h. **(B)** Inclusive intersection of all upregulated genes after addition of supernatant (+ Sup.) vs. at least one other condition (Overlap) or the combination of all molecules (+ Sup. / + Comb.). **(C)** Log_2 fold change of the upregulated genes that are non-intersecting (+ Sup. only) or intersecting among supernatant and at least one other condition (Overlap). Datasets were analyzed by a two-tailed *t*-test. #, $p < 0.0001$. **(D)** UpSet plot of exclusive intersections of upregulating genes between addition of *S. aureus* supernatant and the indicated molecules. (See **Fig. S6** for full UpSet plot of

all intersections.) **(E)** Model of *P. aeruginosa* sensing of *S. aureus* exoproducts. *S. aureus* secretes staphylopine, iron chelators, intermediate metabolites, and possibly proteinaceous molecules that are sensed by *P. aeruginosa*. In response, *P. aeruginosa* upregulates metal starvation and metabolite uptake pathways, which includes production of its own metal-binding molecules pseudopaline and pyoverdine.